Cancer Letters 443 (2019) 91–107

Contents lists available at ScienceDirect

Cancer Letters

journal homepage: www.elsevier.com/locate/canlet

Original Articles

PLK4 is a determinant of temozolomide sensitivity through phosphorylation of IKBKE in glioblastoma

Zuoxin Zhang[a,1], Zengguang Wang[c,1], Kai Huang[a], Yanwei Liu[d], Cheng Wei[a], Junhu Zhou[a], Wei Zhang[d], Qixue Wang[a], Hao Liang[a], Anling Zhang[a], Guangxiu Wang[a], Yingwei Zhen[b,**], Lei Han[a,*]

[a] Tianjin Neurological Institute, Key Laboratory of Post-Neuroinjury Neuro-repair and Regeneration in Central Nervous System, Ministry of Education and Tianjin City, Tianjin Medical University General Hospital, Tianjin, 300052, China
[b] Department of Neurosurgery, The First Affiliated Hospital of Zhengzhou University, Zhengzhou, Henan, 453002, China
[c] Department of Neurosurgery, Tianjin Medical University General Hospital, Tianjin, 300052, China
[d] Department of Neurosurgery, Beijing Tiantan Hospital, Capital Medical University, Beijing, 100070, China

ARTICLE INFO

Keywords:
Glioma
Chemosensitivity
Kinase
PLK4

ABSTRACT

Despite the clinical success of temozolomide (TMZ), its sensitivity remains a major challenge in glioblastoma (GBM). Here, we show that PLK4 affects TMZ sensitivity by regulating the IKBKE/NF-κB axis. The mRNA level of PLK4 was significantly associated with glioma grade progression and inversely correlated with overall survival (OS) in patients with high-grade gliomas (HGG). Further analyses indicated that GBM patients with low PLK4 expression levels gained greater survival benefits from chemotherapy than did those with high PLK4 expression. In GBM cells, TMZ sensitivity was decreased by ectopic expression of PLK4 and enhanced by depletion of PLK4. In the GBM mice model, inhibiting PLK4 in combination with chemotherapy slowed tumor growth and provided a significant survival benefit. Furthermore, PLK4 interacted with and phosphorylated IKBKE, leading to an increase in NF-κB transcriptional activity and anti-apoptosis. Notably, the PLK4 inhibitor CFI400945, which is currently in clinical trials, had a synergistic effect with TMZ, increasing TMZ sensitivity in xenografts from patient-derived primary GBMs. Our work describes the PLK4-IKBKE signaling axis that influences GBM proliferation and chemosensitivity, and can enhance the anti-tumor effects of chemotherapy via therapeutic targeting.

1. Introduction

Glioblastoma (GBM) is one of the deadliest primary malignant brain cancers, with poor survival and remarkably high tumor heterogeneity [1]. The current standard of treatment is maximum surgical resection followed by radiotherapy with concomitant and adjuvant chemotherapy [2]. Irrespective of molecular subclassification, nearly all GBM patients are treated with radiation and temozolomide (TMZ) [3]. However, the prognosis of TMZ-treated patients remains dismal, with a median survival of 12.1–14.6 months [4]. Chemosensitivity to TMZ impacts the prognosis of chemotherapy following surgical removal. Therefore, a better understanding of the molecular mechanisms underlying TMZ chemosensitivity may lead to improved clinical outcomes in GBM patients.

Defects in conserved signaling pathways are well known to play key roles in the origins and behavior of essentially all cancers [5]. Proteins constitute the nodes and hubs in the signaling network [6]. Although cancer is a disease of the genome, its molecular manifestation is a dysfunction of pathways at the protein level [7]. Protein kinases regulate the biological activity of proteins by phosphorylation, and deregulation of this process via dysfunctional kinase activity has been identified as a major mechanism by which tumor cells escape normal physiological constraints on survival and growth [8].

The polo-like kinase (PLK) PLK4 is a serine/threonine protein kinase, that contains only one catalytic domain called the polo-box motif at its extreme C terminus, remaining a unique member of the PLK

* Corresponding author. Tianjin Neurological Institute, Tianjin Medical University General Hospital, 154 Anshan Road, Heping district, Tianjin, 300052, China.
** Corresponding author. Department of Neurosurgery, The First Affiliated Hospital of Zhengzhou University, 1 Jianshe Road East, Zhengzhou, Henan, 453002, China.
E-mail addresses: fcczhenyw@zzu.edu.cn (Y. Zhen), superhanlei@hotmail.com (L. Han).
[1] Zuoxin Zhang, and Zengguang Wang contributed equally to this study.

https://doi.org/10.1016/j.canlet.2018.11.034
Received 24 September 2018; Received in revised form 22 November 2018; Accepted 26 November 2018
0304-3835/

family [9]. PLK4 contributes to cell mitosis and DNA damage response via regulating the cell cycle and centriole duplication [10]. Moreover, dysregulation of PLK4 expression causes a loss of centrosome numeral integrity, thereby promoting genomic instability and tumorigenesis [11]. Different functions of PLK4 in carcinoma have also been elucidated. For instance, PLK4 promotes invasion and metastasis through Arp2/3 complex regulation of the actin cytoskeleton in breast cancer [12]. Additionally, PLK4 mediates epithelial-mesenchymal transition (EMT) in neuroblastoma via the PI3K/Akt signaling pathway [13]. In hepatocellular carcinoma, PLK4 might be one of the pivotal tumor suppressor genes, and a loss of its activity contributes to human hepatocarcinogenesis [14]. PLK4 is aberrantly expressed in several cancers, but few studies have explored PLK4 status in glioma, especially GBM.

The fate of damaged cells in response to stress depends on the balance between pro- and anti-apoptotic signals [15]. NF-κB plays a role in this balance. In the canonical NF-κB signaling pathway, the inhibitor of NF-κB (IκB) is phosphorylated by the IκB kinase (IKK) complex and degrade. Subsequently, nuclear transport of NF-κB proteins initiates the downstream transcription of target genes encoding anti-apoptotic proteins [16]. Constitutive activation of NF-κB has been observed in different kinds of cancer, including lymphoma [17], leukemia [18], breast [19], colon [20], liver [21], pancreas [22], prostate [23], and ovarian [24] cancers. Moreover, many anticancer agents induce NF-κB nuclear translocation, which impinges cellular resistance to anticancer agents [25]. Therefore, excessive and prolonged activation of NF-κB has been established as a principal mechanism of tumor chemoresistance [26].

In this study, we demonstrated a critical role of PLK4 in the regulation of TMZ chemosensitivity. Inhibition of PLK4 (by RNAi or CFI400945) synergized with TMZ to inhibit cell growth and enhance TMZ sensitivity *in vitro* and *in vivo*. Furthermore, PLK4 interacted with IKBKE and phosphorylated IKBKE. The phosphorylation of IKBKE by PLK4 resulted in the activation of NF-κB transcriptional activity. These data indicate, for the first time, that PLK4 has an important role in the regulation of NF-κB activity and TMZ chemosensitivity and thus could be an adjuvant therapeutic target in GBM chemotherapy.

2. Materials and methods

2.1. Analysis of gene expression using online databases

We used mRNA expression microarray data for the non-tumor tissues and all tumor grades from the Chinese Glioma Genome Atlas (CGGA) database (http://www.cgga.org.cn). Data from the US National Cancer Institute Repository for Molecular Brain Neoplasia Data (REMBRANDT, http://cainteGrator-info.nci.nih.Gov/rembrandt), the GSE16011 dataset (http://www.ncbi.nlm.nih.gov/geo/query/acc.cgi?acc = GSE16011) and the Cancer Genome Atlas (TCGA) (http://cancergenome.nih.gov) were used to validate the mRNA expression level as the validation platforms. The mRNA expression profiles of PLK4 and the related prognoses of the patients were also analyzed.

2.2. Tumor specimens, cell culture and transfection

All of the primary human glioma specimens were obtained from patients who underwent surgery at the first affiliated hospital of Zhengzhou University, and each sample contained ≥80% tumor cells, as confirmed by microscopic examination. The tissue samples were graded by the neuropathologist in accordance with the World Health Organization (WHO) criteria and stored in liquid nitrogen. The glioma specimens included grade II (22 samples), grade III (10 samples) and grade IV (22 samples). The histology and clinical data of the glioma samples was shown in Table 1. This study was approved by the institutional review boards of the hospitals, and written informed consent was obtained from all patients. The samples were used for the qPCR analysis.

Human U87, U251, and LN229 GBM cell lines, human astrocytes and human HEK293 embryonic kidney cells were obtained from ATCC (American Type Culture Collection, Manassas, VA, USA, passages 5–20) and grown in Dulbecco's modified Eagle's medium (DMEM) supplemented with 10% fetal bovine serum (FBS, Thermo Fisher Scientific, USA). Cell lines were tested using the ATCC cell line authentication service and routinely tested for mycoplasma. U87 cells carrying EGFRvIII mutation named U87EGFRvIII were kindly provided by Dr. H Ren (Harbin Medical University, Harbin, China) and cultured under identical conditions. The U87EGFRvIII cells were confirmed by western blotting. Patient-derived primary GBM cells were obtained from Dr. CS Kang (Tianjin Medical University General Hospital, Tianjin, China). Cells were grown in serum-free medium (DMEM-F12/Neurobasal [1:1 mix] with 1% B27 and 2 mM L-glutamine and supplemented with 20 ng/mL each of eEGF and FGF2). All cells were grown at 37 °C in a humidified atmosphere (95% humidity) with 5% CO_2.

In the knockdown experiment, GBM cells (U87 and LN229) were treated with PLK4-siRNA, IKBKE-siRNA or negative control siRNA (GenePharma, Shanghai, China) using Lipofectamine 3000 (Thermo Fisher Scientific, USA) according to the manufacturer's instructions. siRNAs to deplete endogenous PLK4 [27] and IKBKE [28] were previously described and had the following sequences: PLK4 siRNA#1 sense, ACUCCUUUCAGACAUAUAAGTT; antisense, CUUAUAUGUCU GAAAGGAGU TT; PLK4 siRNA#2 sense, CUAUCUUGGAGCUUUAUA ATT; antisense, UUAUAA AGCUCCAAGAUAGTT; PLK4 siRNA#3 sense, GGUAGUAC UAGUUCACCUATT; antisense, UAGGUGAACUAGUACUA CCAG; negative control sense, UUCUCCGA ACGUGUCACGUTT; antisense, ACGUGACACGUUCGGAGAATT. IKBKE siRNA sense, AUCAUC GAACGGCUAAAUATT; antisense, UAUUUAGCCGUUCGAUGAU GC. Negative control sense, UUCUCCGAACGUGUCACGUTT; antisense, ACGUG ACACGUUCGGAGAATT. The expression plasmids (pCMV-Myc-tagged IKBKE wild type, IKBKE-constitutively active (CA) mutant, IKBKE-dominant negative (DN) mutant, pEGFP-C1-tagged PLK4 wild type, PLK4-CA, PLK4-DN) were kindly supplied by Dr. JQ Cheng (Moffitt Cancer Center, USA) and transfected into cell lines via Lipofectamine 3000. The above plasmids were confirmed by agarose gel electrophoresis and DNA sequence analysis. The knockdown and overexpression efficiency were detected by qPCR and western blotting as described below.

2.3. RNA isolation and quantitative real-time PCR

Total RNA was extracted using TRIzol reagent (Thermo Fisher Scientific, USA) and the RNA (1 μg) was reverse transcribed for the synthesis of cDNA using a GoScript Reverse Transcription system (Promega, USA). The expression status of mRNA was measured on an ABI QuantStudio 3 using GoTaq® qPCR Master Mix (Promega, USA), and the expression of GAPDH was used as an internal control. Briefly, cDNA product (2 μl) was used as a template in a 10 μl PCR system containing 10 μl of GoTaq® qPCR Master Mix and each primer at 0.2 μm. All reactions were performed in duplicate. Amplification protocols were as follows: 95 °C for 10 min; 44 cycles of 95 °C/10 s, 58 °C/10 s, and 60 °C/10 s. The primer sequences were as follows: PLK4 Forward: 5′-GACACCTCAGACTGAAACCGTAC-3′, Reverse: 5′-GTCCTTCTGCAAA TCTTGGC-3’; BCL2-A1 Forward: CAGGCTGGC TCAGGACTATC, Reverse: TGTTCTGGCAGTGTCTACGG; BCL2-L1 Forward: C TGAATC GGAGATGAGAC, Reverse: TGGGATGTCAGGTCACTGAA; MCL1 Forward: GATGATCCATGTTTTCAGCGAC, Reverse: CTCCACAAACCC ATCCC AG; BCL-2 forward: GATTGATGGGATCGTTGCCT, Reverse: GTGTCTTCAATCA CGCGGAA; GAPDH Forward: 5′-GGTGGTCTCCTCT GACTTCAACA-3′, Reverse: 5′-GTTGCTGTAGCCAAATTCGTTGT-3’. Data were analyzed using the relative standard curve method and normalized to GAPDH.

Table 1
Clinical data of glioma patients.

Case ID	Grade	Pathology	Age	Gender	Location
2745106	Grade2	Astrocytoma	47	Male	Right-Temporal lobe
2837274	Grade2	Astrocytoma	46	Female	Right-Frontal lobe
2820798	Grade2	Astrocytoma	35	Male	Left-Frontal lobe and Corpus Callosum
2758859	Grade2	Astrocytoma	54	Female	Left-Frontal and Temporal lobe
2813936	Grade2	Astrocytoma	21	Female	Right-Frontal lobe
2806517	Grade2	Oligodendroglioma	42	Male	Right-Frontal lobe
2783980	Grade2	Astrocytoma	26	Male	Left-Frontal lobe and Corpus Callosum
2818164	Grade2	Astrocytoma	37	Male	Right-Temporal lobe、Basal ganglia and Thalamus
2786864	Grade2	Astrocytoma	7	Male	Right-Lateral Ventricle
2814879	Grade2	Oligodendroglioma	62	Male	Left-Frontal lobe
2824960	Grade2	Oligodendroglioma	66	Male	Left-Temporal lobe
2763226	Grade2	Astrocytoma	22	Female	Right-Temporal lobe and Insula
2802525	Grade2	Oligodendroglioma	49	Female	Both Frontal lobes
2793240	Grade2	Astrocytoma	53	Female	Left-Parietal and Occipital lobe
2786998	Grade2	Astrocytoma	65	Female	Left-Insula and Hippocampus
2779357	Grade2	Oligoastrocytoma	37	Male	Right-Temporal lobe and Insula
2857854	Grade2	Astrocytoma	47	Male	Right-Frontal and Temporal lobe and Insula
2829007	Grade2	Astrocytoma	13	Male	Right-cerebellum
2836776	Grade2	Oligodendroglioma	66	Female	Left-Frontal lobe
2819364	Grade2	Oligodendroglioma	35	Male	Right-Frontal lobe
2802565	Grade2	Oligodendroglioma	36	Female	Left-Frontal lobe
2464233	Grade2	Oligodendroglioma	56	Male	Right-Frontal lobe
2794004	Grade3	Anaplastic-Pleomorphic Xanthoastrocytoma	8	Male	Multiple
1702716	Grade3	Anaplastic- Oligodendroglioma	65	Male	Right-Frontal lobe
2809212	Grade3	Anaplastic- Oligodendroglioma	44	Male	Left-Frontal lobe
2777349	Grade3	Anaplastic- Astrocytoma	13	Male	Left-Frontal and Parietal lobe
2794592	Grade3	Anaplastic- Astrocytoma	46	Male	Right-Frontal and Temporal lobe and Basal ganglia
2800765	Grade3	Anaplastic- Astrocytoma	55	Female	Right-Frontal and Parietal lobe
2804917	Grade3	Anaplastic- Oligodendroglioma	48	Female	Right-Frontal lobe
2823242	Grade3	Anaplastic- Oligodendroglioma	50	Female	Left-Frontal lobe
2804089	Grade3	Astrocytoma & Anaplastic- Astrocytoma	43	Female	Right-Temporal lobe
2819913	Grade3	Oligodendroglioma & Anaplastic- Oligodendroglioma	29	Female	Right-Frontal and Parietal lobe
2753654	Grade4	Glioblastoma	56	Female	Left-Frontal lobe
2823616	Grade4	Glioblastoma	54	Male	Left-Frontal lobe
2112991	Grade4	Glioblastoma	52	Female	Right-Temporal lobe
2744967	Grade4	Glioblastoma	59	Male	Right-Temporal lobe
2846679	Grade4	Glioblastoma	28	Male	Left-Parietal and occipital lobe
2793379	Grade4	Glioblastoma	78	Male	Right-Frontal lobe
2771238	Grade4	Glioblastoma	69	Female	Left-Frontal lobe
2757698	Grade4	Glioblastoma	16	Male	Left-Occipital lobe
2811574	Grade4	Glioblastoma	51	Female	Right-Temporal lobe and insula
2753409	Grade4	Glioblastoma	21	Female	Right-Frontal lobe
2844223	Grade4	Glioblastoma	69	Male	Left-Frontal lobe
2745654	Grade4	Glioblastoma	70	Female	Left-Frontal and Parietal lobe
2816053	Grade4	Glioblastoma	52	Male	Left-Temporal lobe
2749002	Grade4	Glioblastoma	57	Male	Both-Frontal lobes
2795191	Grade4	Glioblastoma	44	Female	Left-Temporal lobe and Basal ganglia
2768553	Grade4	Glioblastoma	58	Male	Right-Temporal lobe and Insula and Basal ganglia
2804704	Grade4	Glioblastoma	46	Male	Left-Frontal lobe and insula
2741147	Grade4	Glioblastoma	55	Male	Both Lateral ventricles and Corpus Callosum
2769121	Grade4	Glioblastoma	43	Male	Left-Temporal lobe
2759450	Grade4	Glioblastoma	53	Male	Right-Parietal and Occipital lobe
2791746	Grade4	Glioblastoma	69	Male	Right-Temporal lobe
2785372	Grade4	Anaplastic- Astrocytoma & Glioblastoma	77	Male	Right-Frontal and Parietal lobe

2.4. Immunoblotting (IB) and immunoprecipitation (IP) analyses

Cells were lysed in RIPA buffer (Pierce, France) containing a protease and phosphatase inhibitor cocktail (Sigma). The protein concentrations of whole cell lysates were measured by a BCA assay kit (Solarbio, China) according to the manufacturer's instructions. The protein lysates (20 μg) were then separated by SDS-PAGE and transferred to polyvinylidene fluoride (PVDF) membranes (Millipore, USA). The membranes were incubated with primary antibodies against PLK4 (1:250 dilution, Abcam, ab2642), IκBα (phospho S36, 1:2500 dilution, Abcam, ab133462), IκBα (1:5000 dilution, Abcam, ab32518), β-actin (1:1000 dilution, Zsbio, TA-09), and GAPDH (1:1000 dilution, Cell Signaling Technology, 97166) overnight at 4 °C, followed by incubation with the corresponding HRP-conjugated secondary antibody. GAPDH was used as a loading control.

For the IP assay, cells were lysed in lysis buffer containing 50 mM Tris-HCl (pH 7.5), 100 mM NaCl, 1% NP40, 5 mM EGTA (pH 7.5), 1 mM EDTA (pH 8.0), 2 mM phenylmethylsulfonyl fluoride, 2 μg/ml aprotinin and leupeptin, 2 mM benzamidine, 10 mM NaF, 10 mM NaPPi, 1 mM sodium vanadate, and 25 mM β-glycerolphosphate. For IP analysis, lysates (1 mg) were precleaned with protein A-protein G (2:1) agarose beads (GE Healthcare, Sweden) at 4 °C for 20 min. After removal of the beads by centrifugation, lysates were incubated with the indicated antibody (1–2 μg) for 3–4 h at 4 °C followed by 1 h incubation with protein A/G agarose beads. The recovered immuno-complexes were washed three times with lysis buffer, resolved by SDS-PAGE and immunoblotted with the indicated antibodies. Detection of the antigen-bound antibody was carried out with the a SuperSignal West Pico Plus chemiluminescent substrate (Thermo Fisher Scientific, USA).

2.5. In vivo kinase assay

For the *in vivo* kinase assay, after serum starvation overnight, HEK293 cells were cotransfected with EGFP-PLK4 CA and either Myc-IKBKE DN or vector. Conversely, HEK293 cells were cotransfected with Myc-IKBKE CA and either EGFP-PLK4 DN or vector. After transfection for 24 h, IKBKE and PLK4 were immunoprecipitated with anti-Myc (for transfected Myc-IKBKE DN, 1–2 μg, Santa Cruz, SC-40) or anti-GFP (for transfected EGFP-PLK4 DN, 1–2 μg, Santa Cruz, SC-9996) antibody, and the immunoprecipitates were separated by SDS-PAGE. Phospho-IKBKE and phospho-PLK4 were detected via pan-phospho-Ser/Thr (1:1000 dilution, Santa Cruz) antibody.

2.6. Proliferation and cell viability assays

We used colony formation and MTT assays to determine cell growth. GBM cell lines were knocked down or overexpressed PLK4 via either siRNA or plasmid. Following incubation for 2 days, the cells were treated with and without increasing doses of TMZ for 72 h and then subjected to MTT and colony formation assays as previously described [29]. For the colony formation assay, 200 cells per well were seeded in 6-well plates and cultured for 2 weeks following transfection for 48 h. The plates were washed, fixed, stained with crystal violet (0.05%), and visualized on an Olympus upright BX53 microscope. Colonies with more than 50 cells were counted to assess the proliferation of cells. For the cell viability assay, cells were seeded at a density of 5×10^3 cells per well in a 96-well plate. Twenty-four hours later, the cells were treated with TMZ at different concentrations for 72 h. Cell viability was assessed using an MTT assay. Cells were then incubated with 20 μL of MTT (5 mg/ml, Sigma) at 37 °C for 4 h. Thereafter, the media were discarded, and 150 μl of dimethyl sulfoxide (DMSO) was added to each well prior to spectrophotometric measurements at 570 nm. Untreated cells were used as a negative control, and each test was repeated in eight wells.

2.7. Luciferase reporter assay

An NF-κB luciferase reporter plasmid (pNFκB-luc) was obtained from Beyotime Biotechnology (Shanghai, China) in order to detect the transcriptional activity of NF-κB. GBM cells were seeded in 96-well plates and transiently transfected with siRNA (5 pmol or 10 pmol) or wild-type plasmid (100 ng or 200 ng) for PLK4 and then with an equimolar amount of pNF-κB-luc plasmid sequentially. The cells were lysed after 48 h of culture, and luciferase activity was measured with a Bright-Glo™ Luciferase Assay System (E2620, Promega, USA) according to the instructions. Each experiment was repeated six times.

2.8. Immunofluorescence assay

For detection of γ-H2AX, cells were seeded on coverslips, transfected with siRNA against PLK4, and 2 days later treated with TMZ (500 μm for U87 cells, 1000 μm for LN229 cells, and 400 μm for U87-EGFRvIII cells). Cells were stained for γ-H2AX 48 h after the initiation of treatment with TMZ. Immunostaining was performed as previously reported [30]. In brief, the cells were grown on glass coverslips (Thermo Fisher Scientific, USA) in 12-well plates and fixed with 4% paraformaldehyde. The coverslips were then incubated in blocking solution, followed by incubation with primary antibodies against pericentrin (1:100 dilution, Abcam, ab4448), NF-κB-p65 (1:100 dilution, Santa Cruz, sc-8008), PLK4 (1:100 dilution, Abcam, ab2642), γ-H2AX (phospho S139, 1:1000 dilution, Abcam, ab26350), and IKBKE (1:100 dilution, Santa Cruz, sc-376114) overnight at 4 °C and then with Alexa Fluor 488 or 594-labeled secondary antibody (Thermo Fisher Scientific, USA). The cell cytoskeleton was stained with α-tubulin (1:100 dilution, Santa Cruz, sc-8035) for 15 min at room temperature and then rinsed with PBS three times. Subsequently, the cell nuclei were stained with DAPI (0.5 μg/ml, #4083, Cell Signaling Technology) for 5 min at room temperature and then rinsed with PBS three times. The slides were mounted with an aqueous-based mounting medium (F4680, Sigma) and immediately imaged on an Olympus FV1200 laser scanning confocal microscope.

2.9. Intracranial tumor model construction

All mouse experiments were conducted in accordance with protocols approved by the Tianjin Medical University Animal Care and Use Committee and followed guidelines for animal welfare. Five-week-old female BALB/c-nude mice were purchased from Beijing HFK Bioscience Co., LTD. To create the intracranial tumor model, U87 cells were infected with luciferase lentivirus alone or coinfected with PLK4 shRNA lentivirus (or scrambled lentivirus, Genechem, China). For the knockdown of PLK4, PLK4-specific shRNAs (GTAGATGGTTTGCCTATGT) were packaged into lentivirus. After 2 days of infection, 5×10^5 control or PLK4 knockdown cells (in 3 μl PBS) were injected into the intracranial striatum of nude mice with a stereotactic instrument and a microinfusion pump (Stoelting Co., USA) [31]. A burr hole was positioned 1 mm anterior and 2 mm lateral to the bregma prior to introducing a syringe under stereotactic guidance 3 mm from the skull bone into the striatum. Motorized injection of the cells was performed at a rate of 1 μl/min. The animals were randomly divided into 4 groups, with 12 mice in each group. Starting on day 8 after tumor cell implantation, TMZ (5 mg/kg, i.p.) was given to the TMZ and cotreatment groups on a 5 days on/2 days off regimen for 2 cycles [32]. Other animals were treated with an equal volume of DMSO alone. To acquire tumor growth status in live animals of different treatment groups by bioluminescent imaging, the mice were anesthetized and injected intraperitoneally with D-luciferin (150 mg/kg, beetle luciferin, potassium salt, E1605, Promega) 15 min prior to imaging with the IVIS imaging system (perkinelmer, USA) for 10–120 s. Three weeks postimplantation, three animals from each group were sacrificed, and the brain samples were taken for hematoxylin and eosin (HE) staining. The remaining mice in each group were used for bioluminescent imaging and survival analysis. The percentage tumor growth inhibition (% TGI) was defined according to previous methods [33].

2.10. Subcutaneous and orthotopic patient-derived xenografts

Patient-derived GBM cells were provided by Dr. CS Kang. For the subcutaneous model, 5×10^5 cells were suspended in 50 μL of PBS and implanted into the flanks of nude mice. When the tumor volume reached 100 mm^3, the animals were randomized into three groups with 6 mice in each group: negative controls (NC), chemotherapy (TMZ) and combination (CFI400945 and TMZ). CFI400945 (7.5 mg/kg) and the vehicle (water) were administered once daily by oral gavage for 21 days [34], and TMZ and the vehicle (DMSO) were administered to mice by intraperitoneal injection as mentioned above. Tumor volume (mm^3) was measured three times per week and defined as follows: length × $width^2/2$. Three weeks postinjection, the mice were sacrificed, and the tumor tissue was removed for immunohistochemical (IHC) analysis as described below.

For orthotopic transplantation, patient derived GBM cells were infected with the luciferase lentivirus (GenePharma, China). Prior to injection, cells were resuspended in PBS. To generate orthotopic tumors, 20×10^4 cells were stereotactically injected into the brains of nude mice in a total volume of 3 μl with the previously described stereotactic instrument. One week after tumor cell implantation, animals were randomized into three groups with 10 mice in each group: negative controls (NC), chemotherapy (TMZ) and combination (CFI400945 and TMZ). Bioluminescent imaging and survival analyses were carried out as described above. Three weeks postimplantation, three animals from each group were sacrificed, and the brain and major organ samples were taken for HE staining as described below.

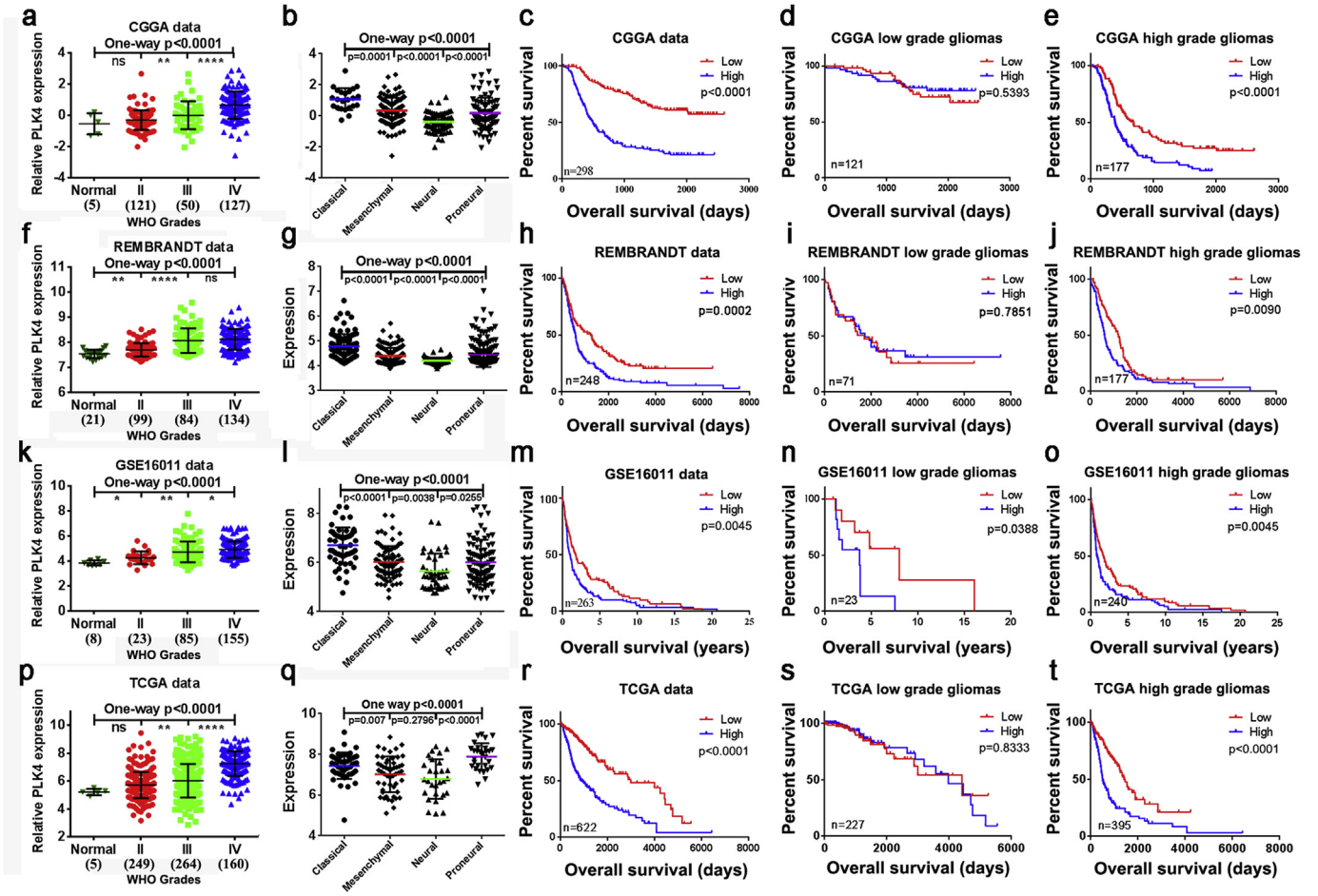

Fig. 1. PLK4 expression signature in the CGGA and validation cohorts and evidence that PLK4 confers poor prognosis in glioma patients. The levels of PLK4 were analyzed in non-tumor brain and glioma tissues of different grades (a) and subtypes (b) in the CGGA cohort. A Kaplan-Meier survival curve was used to examine the relationship between expression of PLK4 and the survival of patients with all gliomas (c), low grade gliomas (d), and high grade gliomas (e) in the CGGA cohort. The levels of PLK4 were analyzed non-tumor brain and glioma tissues of different grades (f) and subtypes (g) in the REMBRANDT cohort. A Kaplan-Meier survival curve was used to examine the expression of PLK4 on the survival of patients with all gliomas (h), low grade gliomas (i), and high grade gliomas (j) in the REMBRANDT cohort. The levels of PLK4 were analyzed in non-tumor brain and glioma tissues of different grades (k) and subtypes (l) in the GSE16011 cohort. A Kaplan-Meier survival curve was used to examine the expression of PLK4 on the survival of patients with all gliomas (m), low grade gliomas (n), and high grade gliomas (o) in the GSE16011 cohort. The levels of PLK4 were analyzed in non-tumor brain and glioma tissues of different grades (p) and subtypes (q) in the TCGA cohort. A Kaplan-Meier survival curve was used to examine the expression of PLK4 on the survival of glioma patients with all gliomas (r), low grade gliomas (s), and high grade gliomas (t) in the TCGA cohort.

2.11. HE and IHC staining

To conduct histological analysis, tumor tissues were fixed in 10% neutral buffered formalin for HE staining and IHC analysis. For IHC analysis, 5 μm slides were dewaxed in xylene and then rehydrated through graded alcohols to distilled water (dH_2O). Antigen retrieval was performed using sodium citrate (pH = 6) buffer at 97 °C for 20 min. Slides were then washed in PBS prior to incubation in 3% H_2O_2 for 5 min to block endogenous peroxidases. After washing in PBS, slides were blocked with blocking serum for 30 min at room temperature. Next, the slides were incubated at 4 °C overnight in a 1:100 dilution with primary antibodies against IκBα (1:100 dilution, Abcam, ab32518), BCl-2 (1:100 dilution, Zsbio, ZM-0010), NF-κB p65 (1:100 dilution, Santa Cruz, sc-8008), γ-H2AX (phospho S139, 1:1000 dilution, Abcam, ab26350) and Ki67 (1:100 dilution, Zsbio, ZA-0502) before being incubated with a biotin-labeled secondary antibody (1:100 dilution) for 1 h at 37 °C, followed by incubation with ABC-peroxidase and diaminobenzidine (DAB). The slides were then counterstained with hematoxylin and mounted. For HE staining, the 5 μm slides were deparaffinized and brought through a graded ethanol series to dH_2O before the nuclei were stained with hematoxylin; the sections were then rinsed in running tap water and stained with eosin before being dehydrated and mounted. Pictures were taken using an Olympus upright BX53 microscope with Olympus UPlanFL 10 × /0.30 objectives (Olympus). CellSens Entry software equipped with a digital CCD camera (Olympus DP22) was used. All experiments were performed independently at least 3 times.

2.12. Histopathologic study in vivo

Three weeks postinjection, three animals from each group were sacrificed, and organic samples were obtained from the heart, liver, spleen, lung, and kidneys. All the samples were preserved in 4% buffered formaldehyde and were subsequently embedded in paraffin. Then, paraffin sections were stained with HE for histopathologic examination via an Olympus upright BX53 microscope. All experiments were performed independently at least 3 times.

2.13. Statistical analyses

A *t*-test was used to determine differences in each 2-group comparison. One-way ANOVA was used to test for differences among at

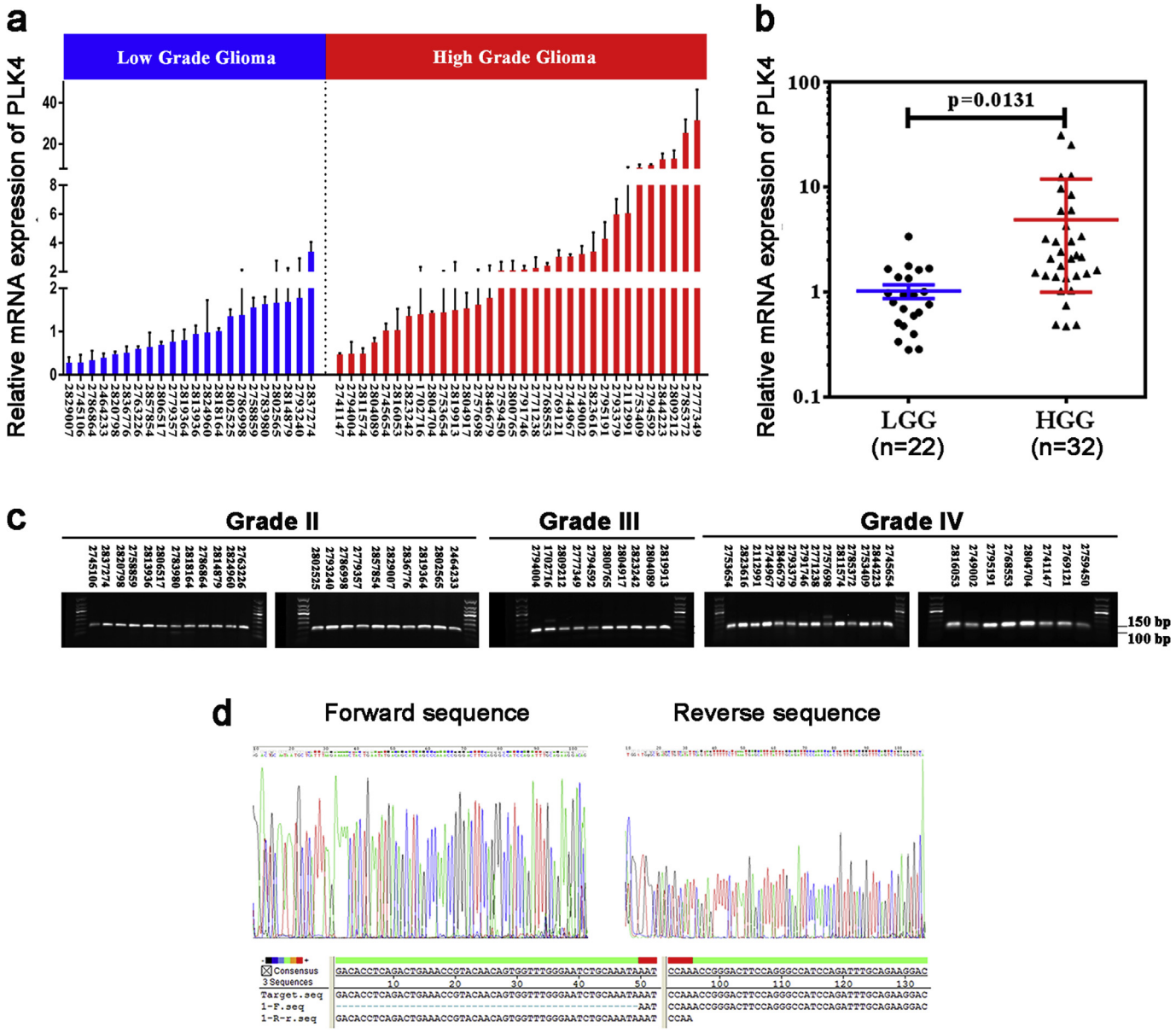

Fig. 2. The expression of PLK4 mRNA was verified in glioma samples. (a)(b) PLK4 mRNA expression levels were detected by qRT-PCR in 54 glioma cases. The sizes and sequences of reaction products were analyzed through agarose gel electrophoresis (c) and Sanger sequencing (d).

least 3 groups, and a least significant difference post hoc test was used to obtain individual p values following ANOVA. Differences in survival were assessed using the Kaplan–Meier method and analyzed using the log-rank test in the univariate analysis. The median values were used as cut-off scores to discriminate between high and low PLK4 expression. Heat maps were constructed using Gene Cluster 3.0 and Gene Tree View software. A two-sided p value < 0.05 was regarded as indicative of significance. MATLAB 2009 software (Pearson correlation) was used to identify the PLK4-related genes. To determine functional gene sets, gene set enrichment analyses were performed using a comprehensive set of functional annotation tools (The Database for Annotation, Visualization and Integrated Discovery, DAVID). All data are presented as the mean ± standard error. All tests were two-sided, and p values < 0.05 were considered to indicate statistical significance.

3. Results

3.1. Gene profiling identifies correlation of PLK4 expression with grade and prognosis in glioma patients

To investigate the expression profile of PLK4 in gliomas, the CGGA cohort, which includes 5 non-tumor brain and 298 glioma samples, was the first to be analyzed. Of 298 gliomas, 121 (40.6%) were WHO II, 50 (16.8%) were WHO III, and 127 (42.6%) were WHO IV. PLK4 expression was found to be significantly downregulated in WHO II glioma patients compared with that in WHO III and WHO IV patients. Moreover, there was also a significant difference in PLK4 expression levels between grade WHO III and WHO IV (Fig. 1a). These findings provided provocative evidence that PLK4 mRNA expression was positively correlated with glioma grade. Based on the CGGA cohort, we then used Kaplan-Meier survival curves and the log-rank method to further analyze the correlation between PLK4 and overall survival (OS). Glioma samples expressing higher than median levels of PLK4 were associated with decreased survival relative to those with PLK4 levels lower than

median levels in the CGGA database (Fig. 1c). Furthermore, PLK4 expression was inversely correlated with OS in high-grade gliomas (HGG) (Fig. 1e). Moreover, PLK4 expression was not inversely correlated with OS in low-grade gliomas (LGG) (Fig. 1d).

To further verify PLK4 expression across the gliomas of each WHO grade, we also conducted a similar analysis for the glioma patients in the REMBRANDT, GSE16011, and TCGA cohorts. These results were consistent with the findings from the CGGA cohort (Fig. 1f, k, and p). Interestingly, further analysis using CGGA and TCGA datasets showed that PLK4 mRNA was consistently down-regulated in the non-tumor brain samples than the gliomas in all grades (Fig. 1a and p). On matching the above datasets, PLK4 mRNA was significantly lower in the non-tumor brain samples than the gliomas in all grades in the REMBRANDT and GSE16011 datasets (Fig. 1f and k). These results implied that elevated PLK4 mRNA expression is associated with genesis and progression of gliomas. The prognostic effect of PLK4 enrichment was also supported by these cohorts (Fig. 1h–j, m-o, and r-t). Overall, our results indicated that high levels of PLK4 were significantly associated with OS in glioma patients and HGG patients and remained increased in HGG patients.

3.2. PLK4 is a marker for glioma molecular subtype

The TCGA described a robust gene expression-based molecular classification of GBM into classical, mesenchymal, neural, and proneural subtypes [35]. To address whether PLK4 expression might distinguish among GBM subtypes, we applied the TCGA classification system to the CGGA (Fig. 1b), REMBRANDT (Fig. 1g), GSE16011 (Fig. 1l), and TCGA (Fig. 1q) cohorts and annotated the samples according to the four TCGA subtypes using the prediction analysis of microarray classifiers as previously described [36]. One-way ANOVA analysis indicated a significant difference in PLK4 expression between the four GBM subtypes in the four cohorts. PLK4 expression in the neural or mesenchymal subtypes was much lower than that in the classical or proneural subtypes in all four datasets. The neural or mesenchymal subtype-specific expression of PLK4 in GBM, which was consistent among the four cohorts, suggested that PLK4 might be involved in the clinical prognosis and therapeutic response of specific subtypes of GBM.

3.3. Verification of PLK4 expression in human glioma samples

In the present study, 22 grade II samples, 10 grade III samples and 22 grade IV samples were collected for further confirmation of different PLK4 expression levels. Consistent with the cohort data described above, the level of PLK4 mRNA was significantly increased in HGG samples compared to LGG samples (Fig. 2a and b). To confirm whether the conclusions drawn from the qPCR analysis were reliable, the gene size and sequences of the PCR products were evaluated by agarose gel electrophoresis (Fig. 2c) and Sanger sequencing (Fig. 2d), respectively. These results indicated that PLK4 might be involved in glioma carcinogenesis and progression.

3.4. PLK4 is a proliferation and DNA damage repair-associated protein kinase

To identify the function of PLK4 involvement in glioma, Pearson correlation and cluster analysis were performed on the CGGA cohort data according to the expression pattern of PLK4. A heatmap indicated that a large number of genes were positively or negatively correlated with PLK4 (Fig. 3a); thus, we screened and evaluated these genes showing an association with PLK4 ($|r| > 0.5$, $P < e^{-21}$). Kyoto Encyclopedia of Genes and Genomes (KEGG) pathway analysis revealed that PLK4 was highly correlated with proliferation and DNA repair pathways (Fig. 3b). The biological processes identified included cell cycle phase, mitosis, nuclear division and DNA repair (Fig. 3c), while the cellular component chart further showed that the PLK4-associated genes were mainly located in the nucleus, centrosome, and chromosome (Fig. 3d). These analyses revealed that PLK4-regulated genes were primarily associated with DNA repair, cell division, DNA replication, and mitotic nuclear division.

In the CGGA cohort, the patients who received standard therapy achieved the best OS and progression-free survival (PFS), and the patients with primary GBMs (pGBMs) who received only radiotherapy exhibited the worst survival (Fig. 3e and f). To further explain this phenomenon, we postulated an association between PLK4 expression and therapeutic outcome, divided the patients into high-expression and low-expression groups and then further subdivided these groups into TMZ-treated and non-TMZ-treated subgroups. We found that the patients in the PLK4 low-expression group were perfectly separated, indicating that the patients who accepted standard therapy experienced longer OS (Fig. 3g) and PFS (Fig. 3h) than the patients who received only radiotherapy; however, this same phenomenon was not observed in the PLK4 high-expression group (Fig. 3i and j). To underscore the potential for a medication-guiding role for PLK4, we analyzed the effect of PLK4 expression on the prognosis of pGBM patients who received the standard therapy. Kaplan-Meier analysis showed that the OS and PFS of participants displaying low PLK4 expression were significantly longer than those of the PLK4 high-expression participants (Fig. 3k and l). These results indicated that PLK4 might sensitize GBM patients to TMZ chemotherapy.

3.5. PLK4 inhibits GBM cell proliferation and sensitizes GBM cells to TMZ

To validate the above results of the KEGG and Gene Ontology (GO) analyses of PLK4, gain- and loss-of-function assays were performed to assess the molecular role of PLK4 in GBM. Initially, reverse transcription quantitative PCR (RT-qPCR) was performed to examine PLK4 mRNA expression in GBM cell lines, including U251, LN229, U87, and U87EGFRvIII cells, as well as in human astrocytes. The human astrocytes expressed low levels of PLK4 and were used as a normal control. For the other four GBM cell lines, U251 and U87EGFRvIII cells expressed lower PLK4 levels than LN229 and U87 cells (Fig. 4a). To address whether PLK4 influenced malignant proliferation and TMZ responses of GBM cells, U87EGFRvIII cells were transfected with a PLK4 overexpression plasmid, while LN229 and U87 cells were transfected with three siRNAs against different regions of PLK4. qPCR and western blotting were performed, and the results showed that the mRNA and protein levels of PLK4 were significantly upregulated in PLK4 plasmid-transfected U87EGFRvIII cells compared with those in the control cells, while the mRNA and protein levels of PLK4 were significantly knocked down in PLK4-siRNA transfected LN229 and U87 cells compared with those in control cells (Fig. 4b and c). siRNA #2 and #3 showed higher efficiency and were thus used in subsequent analyses. PLK4 has emerged as a central, upstream regulator of centriole biogenesis in many cells, including glioma cells. Therefore, centriole immunofluorescence staining was used to further prove that our knockdown and overexpression systems were reliable. As expected, ectopic PLK4 expression in U87EGFRvIII cells significantly elevated the frequencies of centrosome amplification. Conversely, PLK4 knockdown (siRNA #2) in LN229 and U87 cells inhibited centrosome amplification. The results confirmed that the PLK4 overexpression and knockdown system worked efficiently (Fig. 4d).

MTT and colony-formation assays showed that the growth of LN229 and U87 cells transfected with siRNAs (#2 and #3) decreased markedly (Fig. 4e, f, h, and i). Moreover, U87EGFRvIII cells transfected with a PLK4 overexpression plasmid manifested significant cell proliferation promotion *in vitro* (Fig. 4g and j). Based on previous studies in the CGGA cohort, GBM patients with low PLK4 levels showed a stronger association with a better clinical outcome from TMZ therapy than those with high PLK4 expression (Fig. 3g, h, i, and j). Thus, we then asked whether PLK4 could modulate the sensitivity of GBM cells to TMZ. As

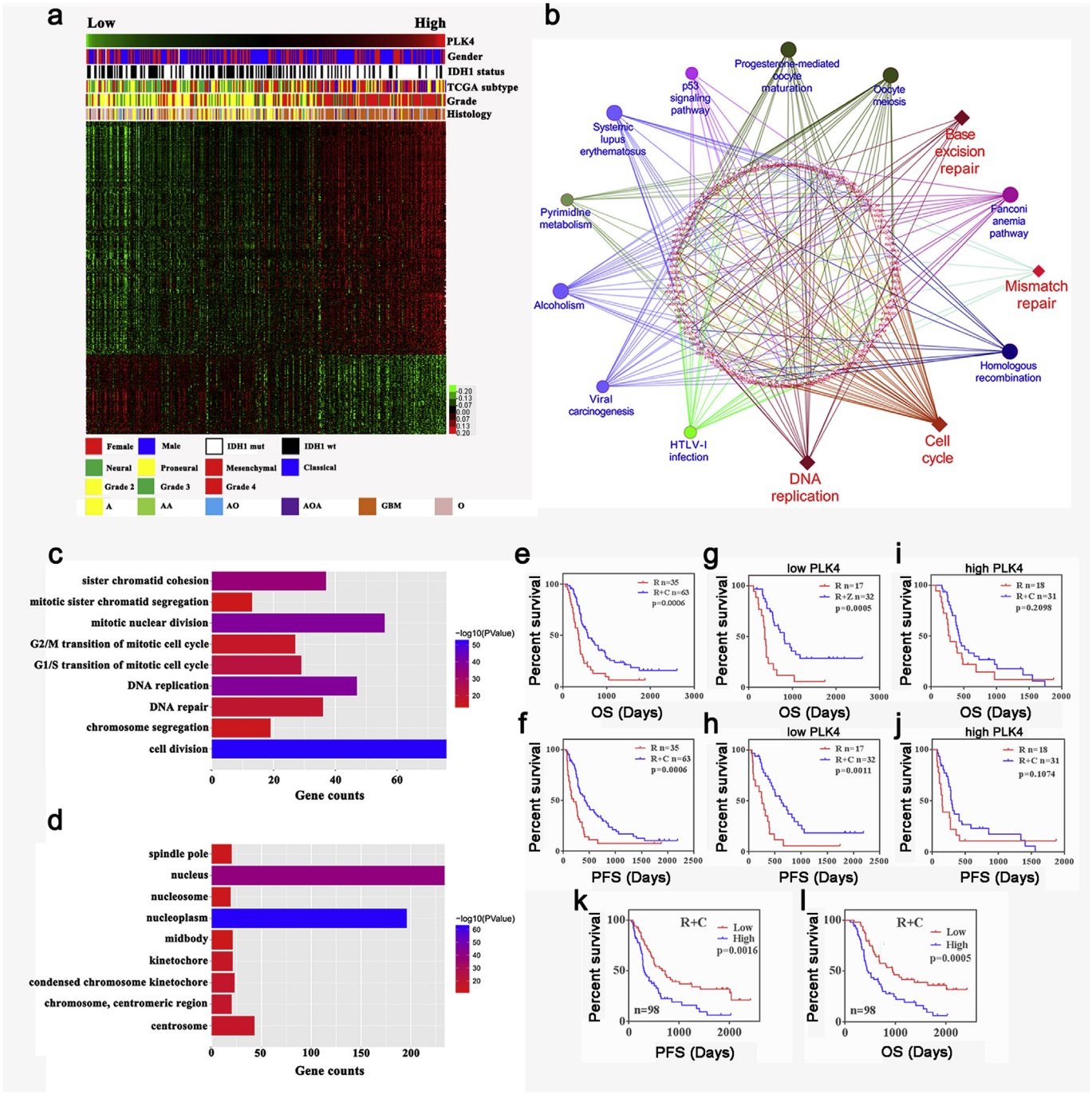

Fig. 3. The PLK4-associated genes were chiefly enriched in proliferation- and DNA damage repair-related pathways. (a) Correlation analysis was performed on 298 samples with mRNA microarrays from the CGGA cohort. A heatmap of the relative expression levels of PLK4-associated genes in glioma tissues sorted by the level of PLK4 expression is shown. (b) A KEGG pathway network was constructed using the PLK4-associated genes. An analysis of biological processes (c) and cellular components (d) was performed using the PLK4-associated genes; this information was obtained from the GO database. Overall survival (OS) (e) and progression-free survival (PFS) (f) of all of the primary GBM patients who received combined chemotherapy and radiotherapy were longer than those of patients who received only radiotherapy. The OS (g) and PFS (h) were longer in participants who received combined chemotherapy and radiotherapy and who displayed low PLK4 mRNA expression than in participants with high PLK4 expression who did not. The OS (i) and PFS (j) of participants who received combined chemotherapy and radiotherapy and displayed high PLK4 mRNA expression were not significantly longer than those in participants who received only radiotherapy. All participants received TMZ treatment. The PFS (k) and OS (l) of participants displaying low PLK4 mRNA expression were found to be longer than those of participants with high expression levels. All values were acquired from the CGGA cohort.

expected, the combination of PLK4 knockdown and TMZ presented an enhanced antitumor effect compared with TMZ alone. In a profound dose-response analysis of GBM cells, we confirmed that the IC50 values of TMZ in U87, LN229, and U87-EGFRvIII cells were 943.9 μM, 2126.8 μM, and 632.9 μM, respectively. The presence of PLK4 knockdown effectively restored sensitivity to TMZ, and IC50 values were decreased to 423.9 (si#2)/352.9 (si#3) μM and 839.0 (si#2)/1184.9 (si#3) μM in U87 and LN229 cells, respectively (Fig. 4k and l). Conversely, the PLK4-overexpressing U87EGFRvIII cells exhibited resistance to TMZ, with IC50 values increasing to 1878.8 μM (Fig. 4m).

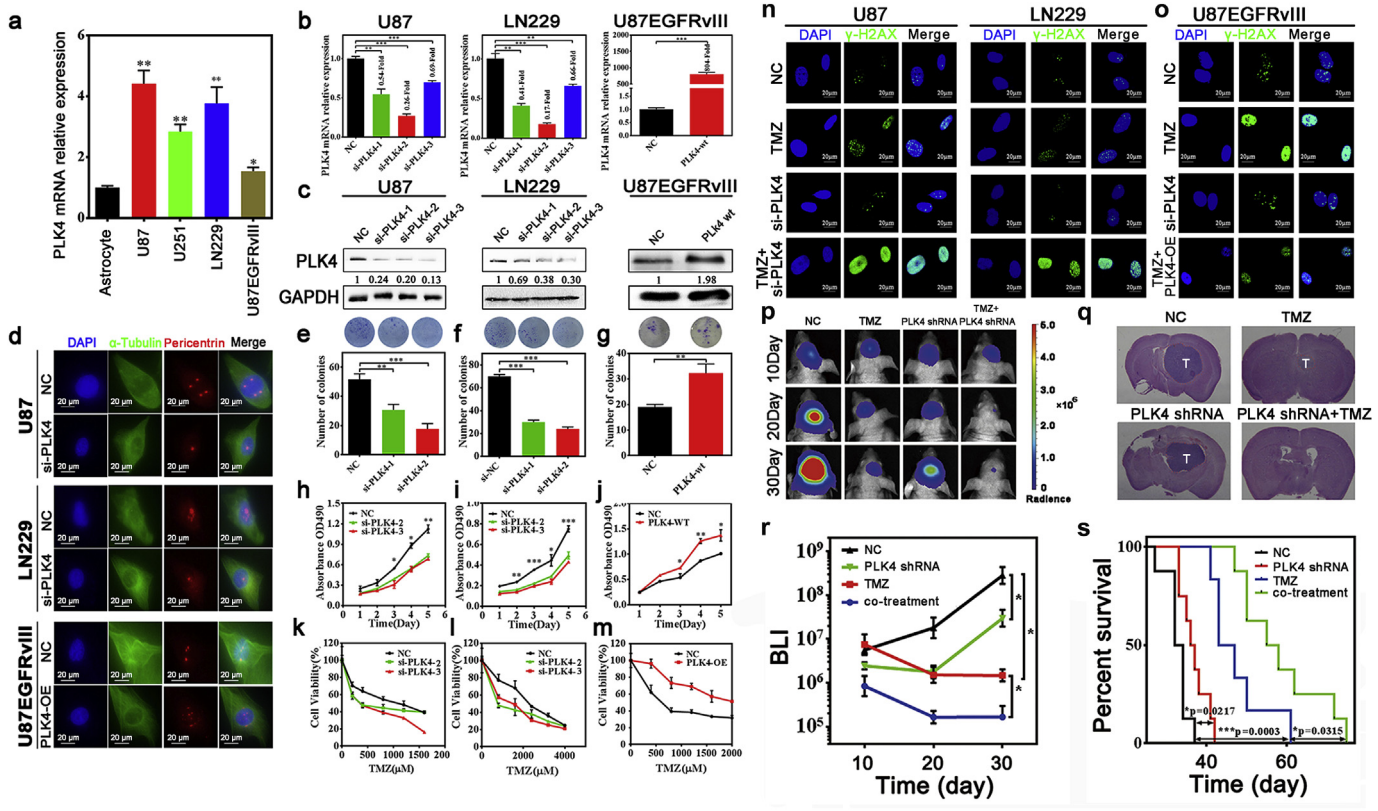

Fig. 4. PLK4 regulates glioma growth and chemosensitivity *in vitro* and *in vivo*. (a) Expression of PLK4 was determined in GBM and human astrocyte cell lines by qRT-PCR. Expression levels are shown relative to the expression in human astrocyte cells, which was used as a control and set as 1. qPCR (b) and western blotting (c) panels represent PLK4 expression in U87, LN229, and U87EGFRvIII cells infected with PLK4 siRNAs or expression plasmids for wild-type PLK4. (d) Immunofluorescence staining for centriole-associated markers in PLK4 overexpressing or knockdown GBM cells. U87 (e)(h) and LN229 (f)(i) cells were transfected with two siRNAs of PLK4 or control siRNA. U87EGFRvIII cells (g)(j) were transfected with overexpression plasmid for PLK4 or control plasmid vector. Total cell proliferation ability was assessed by colony formation (e–g) and MTT assays (h–j). PLK4 siRNA-treated U87 (k), LN229 (l), and PLK4 overexpression plasmid-treated U87EGFRvIII cells (m) were treated with and without TMZ. Total cell viability was assessed by MTT assays. Experiments were repeated three times, and each experiment was performed in six repeats. (n) Immunofluorescence of γ-H2AX foci in PLK4 knockdown U87 and LN229 cells after treatment with TMZ for 48 h. (o) Immunofluorescence of γ-H2AX foci in PLK4 overexpression U87EGFRvIII cells after treatment with TMZ for 48 h. Bioluminescent images (p) and bioluminescent intensity (r) of the glioma-bearing mice 10, 20, and 30 days after treatment with TMZ, lenti-PLK4 knockdown or cotreatment with TMZ and lenti-PLK4. (q) Images of HE staining of the full-brain sections (the normal tissue and tumor tissue are separated by the dashed line), dissected at day 21 after tumor implantation and treated with TMZ, lenti-PLK4 knockdown or cotreatment with TMZ and lenti-PLK4. (s) Survival rate of the glioma-bearing mice after treatment with TMZ, lenti-PLK4 knockdown or cotreatment with TMZ and lenti-PLK4. The asterisks denote significance (*$p < 0.05$, **$p < 0.01$, and ***$p < 0.005$).

Table 2
Effect of treatment on tumor growth inhibition, mean survival days, median survival time, and percentage increase in life span.

Groups	Tumor Growth Inhibition (TGI% on day 30)	Mean Survival (Days)	Median Survival Time (MST) (Days)	Percentage Increase in Life Span (ILS%) (Days)
Negative control	n/a	32.8 ± 2.7	33	/
PLK4 shRNA	89.4 ± 4.75	36.9 ± 3.1	36.5	10.6
TMZ	99.5 ± 0.15	47.5 ± 6.7	45	36.4
TMZ + PLK4 shRNA	100 ± 0.03	58.6 ± 9.7	56.5	71.2

Given the above findings, we next examined whether PLK4 depletion enhances the DNA damage conferred by TMZ. PLK4-depleted cells treated with TMZ showed a significant increase in γ-H2AX foci compared with cells treated with TMZ or siPLK4 (#2) alone (Fig. 4n). Conversely, PLK4 overexpression mitigated the ability of TMZ to induce DNA damage in U87EGFRvIII cells (Fig. 4o). Together, these results suggest that PLK4 silencing enhances persistent DNA break-associated nuclear foci after exposure to TMZ.

We then further validated the function of PLK4 in an *in vivo* orthotopic model using U87 cells expressing the bioluminescent reporter luciferase. The progression of the tumors was quantified by their bioluminescent intensity (BLI) (Fig. 4p and r). TMZ or PLK4 knockdown alone had a moderate effect on tumor growth and mouse survival (median survival = 33 days for the control group, 36.5 days for the PLK4 knockdown group, and 45 days for the TMZ group; Fig. 4s and Table 2). However, the combination of TMZ and PLK4 knockdown significantly reduced U87 tumor growth, leading to a significant increase in mouse survival (median survival = 56.5 days). The BLI of the combined TMZ and PLK4 knockdown group was significantly inhibited (~1 order of magnitude lower than that of the TMZ group at day 30). Fig. 4q showed HE staining of the brain sections collected on day 21, further confirming that the combination of TMZ and PLK4 knockdown significantly inhibited progression of the tumor, which was consistent with the bioluminescent imaging. Together, these results suggested that PLK4 might mediate the resistance to TMZ in GBM cells.

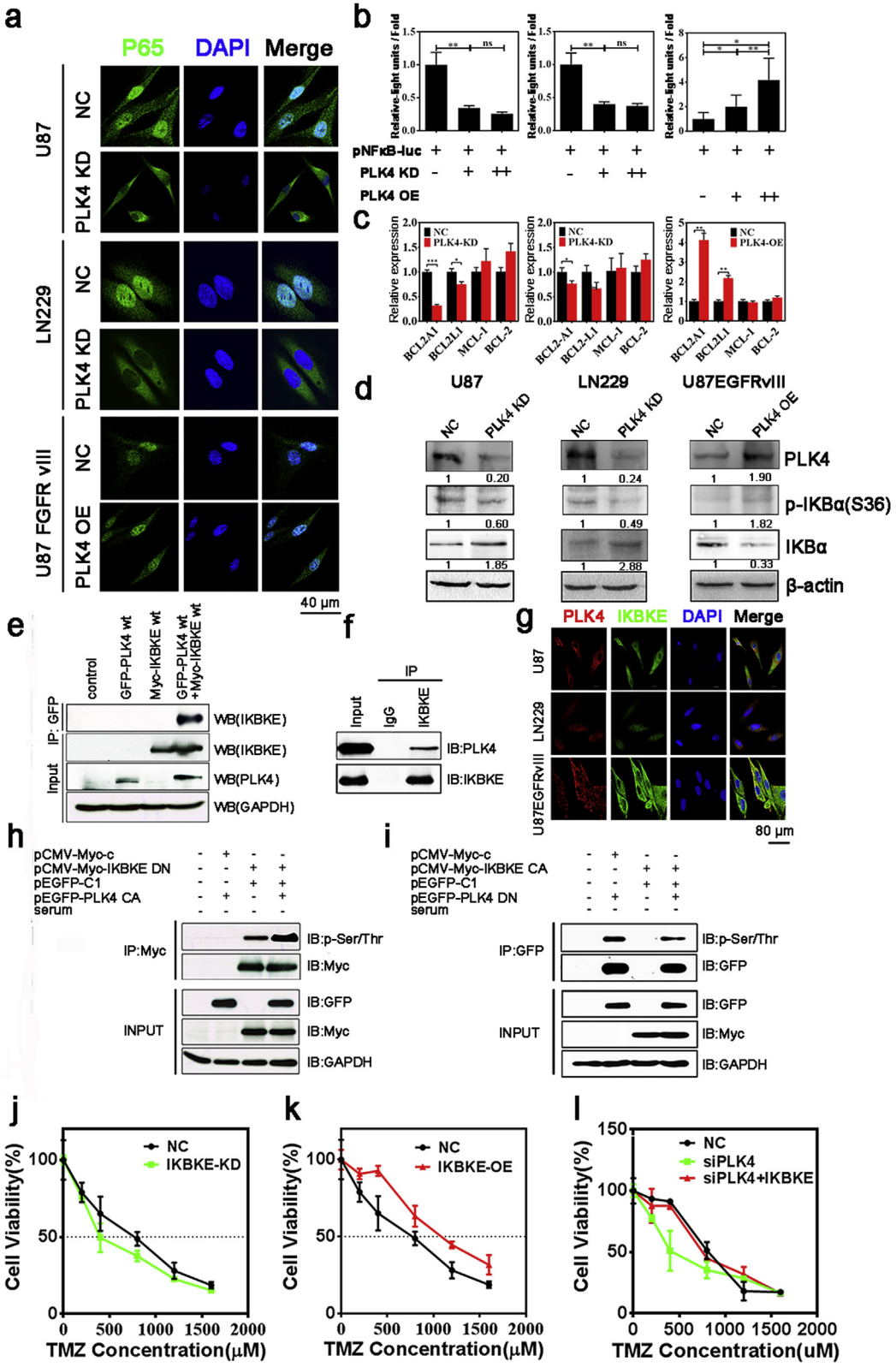

(caption on next page)

3.6. PLK4 induces NF-κB p65 dissociation from IκBα and accumulation in the nucleus and enhances NF-κB p65 target gene transcription

NF-κB, a pro-survival transcription factor, is constitutively activated in a substantial proportion of cancers. The family of nuclear factor NF-κB has 5 cellular members: p105/p50 (NF-κB1), p100/p52 (NF-κB2), p65 (RelA), RelB, and c-Rel. Dominant among these cellular members of the NF-κB transcription factor is the p50/p65 heterodimer. Usually, NF-κB complexes are localized to the cytoplasm, where they bind to IκB inhibitory proteins (IκBα, IκBβ, and IκBε). Upon stimulation, IκB proteins are rapidly phosphorylated by the IKK family and degraded via the ubiquitin-proteasome pathway. NF-κB then translocates to the nucleus

Fig. 5. PLK4 induces NF-κB transactivation and increases chemoresistance via phosphorylation of IKBKE. (a) Immunofluorescence analysis of NF-κB p65 (green fluorescence) intracellular location in GBM cells after PLK4 knockdown or overexpression. The nuclei were counterstained with DAPI (blue fluorescence). (b) Reporter plasmid assays were performed in LN229, and U87 cells transfected with pNFκB-luc plasmid and PLK4 siRNA (#2). Reporter plasmid assays were also performed in U87EGFRvIII cells transfected with pNFκB-luc plasmid and PLK4 overexpression plasmid. Following 48 h of incubation, luciferase activity was measured. The results are presented as the mean ± s.e. of three independent experiments. (c) The mRNA levels of anti-apoptosis family genes in GBM cells transfected with PLK4 siRNA (#2) or overexpression plasmid for 48 h were quantified by qPCR. (d) PLK4, IKBα, and IKBα (phospho S36) protein levels in LN229 and U87 cells transfected with PLK4 siRNA (#2) or in U87EGFRvIII cells transfected with PLK4 overexpression plasmid for 48 h were detected by immunoblotting. (e) HEK293 cells were transfected with Myc-IKBKE and GFP-PLK4 plasmids. After 48 h of incubation, cells were lysed, immunoprecipitated with anti-GFP antibody and immunoblotted with anti-IKBKE antibody (top panel). Panels 2–4 showed the expression of transfected plasmids. (f) For endogenous IKBKE and PLK4 interaction, LN229 cells were immunoprecipitated with anti-IKBKE and detected with anti-PLK4 antibody. (g) Confocal images showed the colocalization of PLK4 (red fluorescence) and IKBKE (green fluorescence) in U87, LN229, and U87EGFRvIII cells. (h)(i) HEK293 cells were transfected with the indicated plasmids. After 48 h of transfection, cells were immunoprecipitated with anti-Myc or anti-GFP antibody and immunoblotted with indicated antibodies. IKBKE siRNA-transfected U87 cells (j), and IKBKE overexpression plasmid-transfected U87 cells (k) were treated with TMZ. (l) U87 cells transfected with PLK4 siRNA, or cotransfected with PLK4 siRNA and IKBKE overexpression plasmid were treated with TMZ. Total cell viability was assessed by MTT assays. The asterisks denote significance (*$p < 0.05$, **$p < 0.01$, and ***$p < 0.005$). (For interpretation of the references to colour in this figure legend, the reader is referred to the Web version of this article.)

and triggers transcription of various targeted genes [37]. As in most human cancers, deregulation of the NF-κB pathway promotes GBM tumor growth and resistance to cytotoxic agents through the transcriptional activation of genes associated with suppression of apoptosis [38,39].

Since MGMT expression is lower in U87 and LN229 cells [40–42], we speculated that PLK4-mediated TMZ resistance was in the MGMT-independent pathway. Previous findings demonstrated that activation of NF-κB conferred chemo-resistance to TMZ in glioblastoma cells [43–46]. Second, it has been demonstrated that IKBKE (an IKK family member) could activate NF-κB transcriptional activity via phosphorylating IκBα [47,48]. Third, predictive analytics revealed that IKBKE might be a potential substrate of PLK4. Therefore, we speculated that PLK4 might dissociate the IκBα/NF-κB complex via phosphorylating IKBKE, thus transferring NF-κB p65 to the nucleus for transcriptional activation. To test this hypothesis, we first assessed the cellular distribution of NF-κB p65 by immunofluorescent (IF) staining. The results showed that the expression of PLK4 induced the localization of NF-κB p65 from the cytoplasm to the nucleus, while knockdown of PLK4 induced the localization of NF-κB p65 from the nucleus to the cytoplasm (Fig. 5a). We then used the NF-κB luciferase reporter assay to explore the possibility that PLK4 enhanced NF-κB p65 transcription activity. As shown in Fig. 5b, the results showed that ectopic expression of PLK4 increased NF-κB p65 reporter activity in U87EGFRvIII cells in a dose-dependent manner. Consistently, specific knockdown of PLK4 via siRNA decreased NF-κB p65 reporter activity in U87 and LN229 cells. To further confirm the above results, changes in the expression levels of antiapoptosis genes regulated by NF-κB were also investigated after PLK4 knockdown or overexpression. Decreased expression of BCL2A1 and BCL2L1 was observed in U87 and LN229 cells. However, upregulation of BCL2A1 and BCL2L1 through PLK4 overexpression was observed in U87EGFRvIII cells (Fig. 5c). Upon stimulation, activation of NF-κB is preceded by phosphorylation and degradation of IκBα. To determine whether PLK4 activates NF-κB, we next determined the expression of IκBα in GBM cells after overexpression or knockdown of PLK4. The results showed that PLK4 could induce the phosphorylation and degradation of IκBα at serine residues (Ser36) (Fig. 5d). These results provide evidence that PLK4 modulates NF-κB pathway activity, which could potentially promote TMZ resistance in GBM cells.

3.7. PLK4 interacts with and phosphorylates IKBKE to activate the NF-κB pathway and induce resistance to TMZ in GBM cells

To determine the mechanism by which PLK4 induced NF-κB transactivation activity, we initially performed co-immunoprecipitation (Co-IP) in HEK293 cells following transfection with GFP-PLK4 and Myc-IKBKE. Fig. 5e showed that Myc-IKBKE interacted with GFP-PLK4. We next examined whether endogenous PLK4 and IKBKE form a complex. Co-IP was carried out in LN229 cells, increased levels of PLK4 and IKBKE [28]. As shown in Fig. 5f, PLK4 was readily detected in IKBKE immunoprecipitates. To determine whether PLK4 colocalized with IKBKE in situ, we performed IF staining in GBM cells and found that PLK4 colocalized with IKBKE in the cytoplasm (Fig. 5g). These data indicated that PLK4 complexed with IKBKE in GBM cells.

We next investigated whether PLK4 phosphorylated IKBKE via an *in vivo* kinase assay. HEK293 cells were cotransfected with EGFP-PLK4 CA and either Myc- IKBKE DN or vector. After transfection for 24 h, IKBKE was immunoprecipitated with anti-Myc antibody, and the immunoprecipitates were separated by SDS-PAGE. Following exposure of an X-ray film, we observed that phosphorylation of IKBKE was induced by PLK4 (Fig. 5h). Conversely, PLK4 could not be phosphorylated by IKBKE (Fig. 5i). The amino acid(s) of IKBKE that were phosphorylated by PLK4 were assessed in our laboratory using GST fusion proteins containing different regions of IKBKE via *in vitro* kinase assay and mass spectrometry. As expected, depletion of IKBKE by siRNA increased the sensitivity of U87 cells to TMZ (Fig. 5j), while overexpression of IKBKE by plasmid increased the resistance of U87 cells to TMZ (Fig. 5k). Furthermore, the enhanced chemosensitivity in PLK4-knockdown U87 cells was diminished by IKBKE overexpression (Fig. 5l).

Taken together, these results indicated that PLK4-mediated TMZ resistance occurred in an IKBKE-dependent pathway. First, PLK4 could complex with and phosphorylate IKBKE. Then, phosphorylated IKBKE could further activate NF-κB transcriptional activity via phosphorylation and degradation of IκBα at serine residues (Ser36). Finally, NF-κB translocated into the nucleus and triggered transcription of various antiapoptosis genes, promoting GBM tumor resistance to chemotherapy.

3.8. CFI-400945 manifests a better therapeutic efficacy combined with TMZ in the PDX model and revealed no obvious side effects on important organs

To validate the PLK4 chemical inhibitors (CFI400945) in a more relevant clinical setting, we injected patient-derived primary GBM cells subcutaneously into nude mice and treated them with orally administered CFI400945 and intraperitoneally administered TMZ. One week after patient-derived primary GBM cell injection, mice received TMZ or a combination of CFI400945 and TMZ for four weeks, and tumors were continuously followed up by caliper measurements (Fig. 6a). Xenografts treated with TMZ alone showed slower tumor growth compared with the control xenografts, but xenografts treated with a combination of CFI400945 and TMZ showed a drastic reduction in tumor volume compared with those treated with TMZ alone at all time points after treatment until the control group reached the four week time point (Fig. 6b and c). Postmortem tumor analysis of xenografts revealed a striking decrease in tumor size and tumor weight in the CFI400945 and TMZ-cotreated tumors compared with those treated with TMZ alone (Fig. 6d and e). To study the molecular mechanisms of treatment *in vivo*, we performed IHC staining in brain samples. Animals treated with TMZ alone showed increased IKBα and γ-H2AX staining compared with the

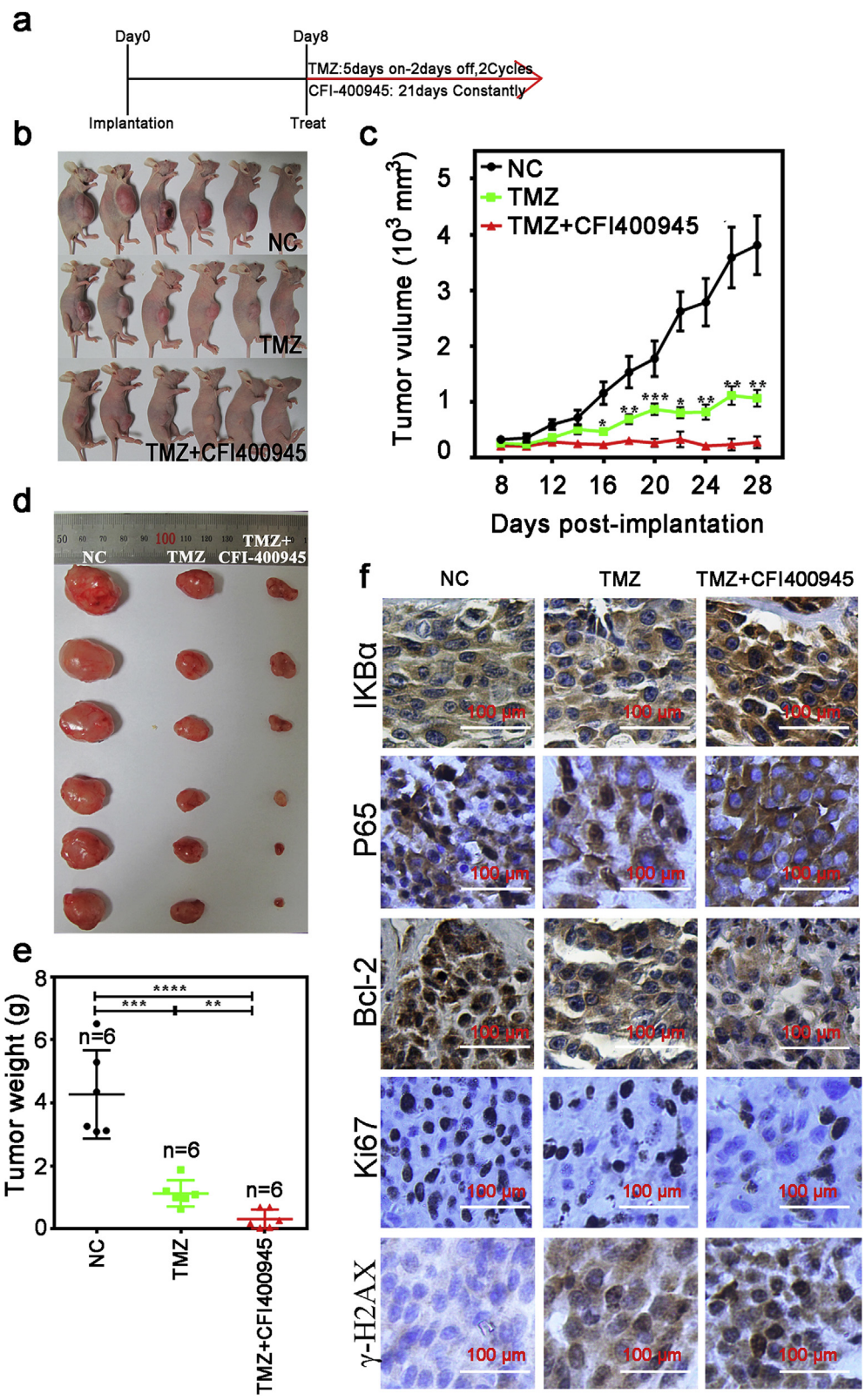

Fig. 6. PLK4 chemical inhibitors sensitized patient-derived primary GBM cells to TMZ in the subcutaneous animal model. (a) Xenograft mouse models from patient-derived primary GBM cells were generated by subcutaneous injection of cells into nude mice. Eight days after injection, mice were treated either with TMZ alone or cotreated with TMZ and CFI400945. Representative image of subcutaneous tumors (b), tumor growth curve (c), dissected tumors (d), and tumor weight (e) in TMZ-treated or cotreated xenograft models with patient-derived primary GBM cells. (f) Representative images of IHC staining for IKBα, p65, Bcl-2, γ-H2AX, and Ki67 in TMZ-treated or cotreated tumors. The asterisks denote significance (*p < 0.05, **p < 0.01, and ***p < 0.005).

control animals, suggesting the effectiveness of TMZ. In contrast, PLK4 KD and TMZ combination induced a significant increase in IKBα and γ-H2AX staining. p65 was almost localized to the nucleus in the control and TMZ groups, while p65 translocated from the nucleus to the cytoplasm in the PLK4 KD and TMZ combination groups (Fig. 6f). These results indicated that CFI400945 treatment increased IKBα stability, p65 cytoplasm accumulation and DNA damage. Moreover, combination-treated animals displayed a significant decrease in Bcl-2 and Ki67 staining compared with animals treated with TMZ alone, indicating possible death by apoptosis. These results indicated that CFI400945 treatment led to TMZ chemosensitivity via blocking IKBα/NF-κB/Bcl-2 axis.

The development of kinase-targeted therapies for central nervous system (CNS) diseases remains a challenge, and the greatest challenge

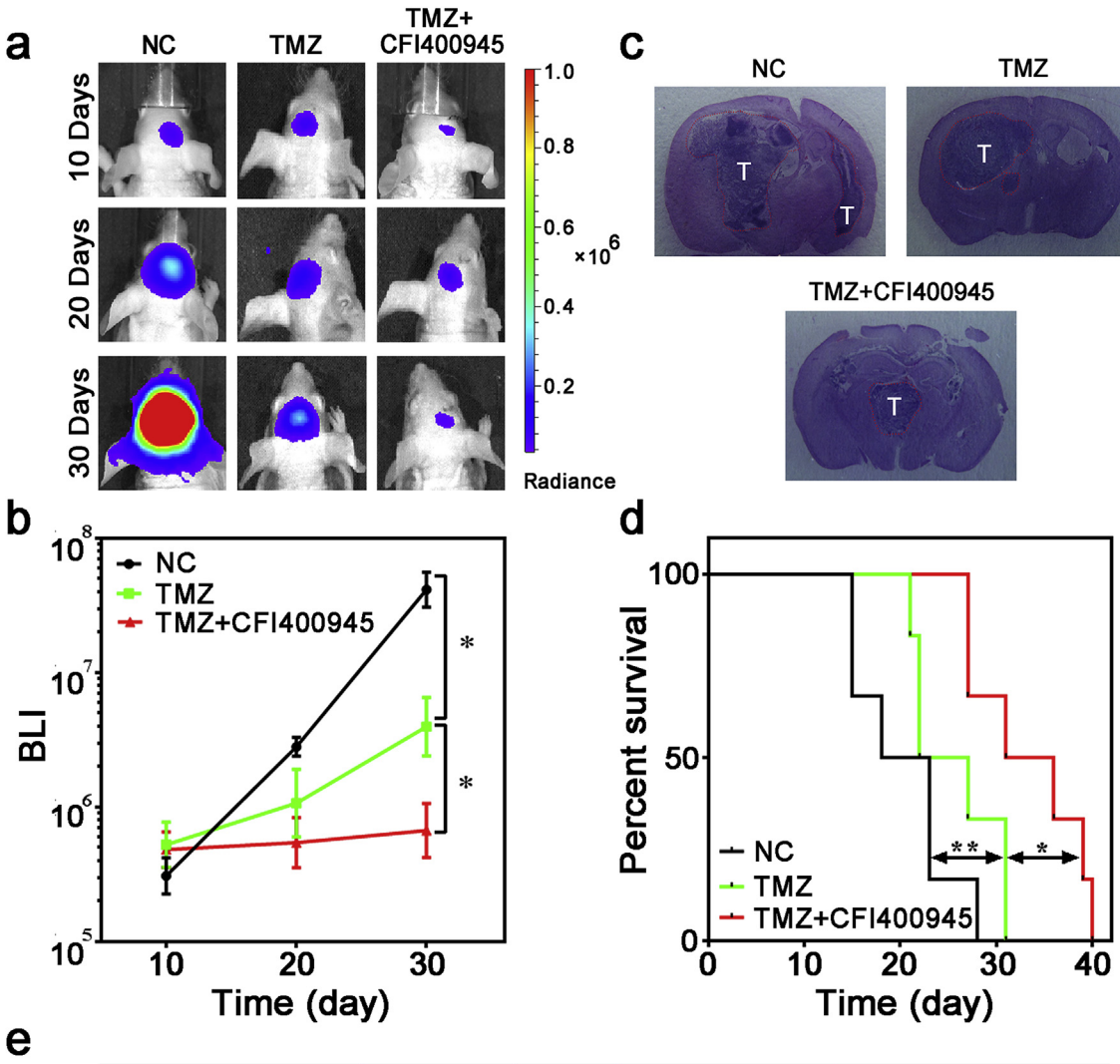

e

Groups	Tumor Growth Inhibition (TGI% on day 30)	Mean Survival (Days)	Median Survival Time(MST)(Days)	Percentage Increase in Life Span(ILS%)(Days)
Negative control	n/a	20.3±4.7	20.5	/
TMZ	90.4±10	25.7±4.2	24.5	19.5
TMZ+CFI400945	98.4±1	31.5±4.6	30	46.3

Fig. 7. PLK4 chemical inhibitors sensitized orthotopic GBM patient-derived tumors to TMZ in mice. *In vivo* bioluminescent (BLI) images (a) and quantitative analysis (b) of GBM xenografts derived from the luciferase-labeled GBM patient-derived cells with the indicated modifications. (c) Images of HE staining of the full-brain sections, dissected at three weeks after tumor implantation and treated with TMZ, or combination of TMZ and CFI400945 (the normal tissue and tumor tissue are separated by the dashed line). (d) Kaplan-Meier survival analysis of mice bearing orthotopically transplanted patient-derived GBM cells. Group 1: treated with vehicle. Group 2: treated with TMZ alone (5 mg/kg, i.p. injection). Group 3: cotreated with TMZ and CFI400945 (7.5 mg/kg, oral gavage). (e) Effect of treatment on tumor growth inhibition (TGI% on day 30), mean survival days, median survival time (MST), and percentage increase in life span (ILS%) of brain tumor bearing mice. The asterisks denote significance (*$p < 0.05$, and **$p < 0.01$).

facing these therapies is the effective penetration of the blood-brain barrier (BBB) [49]. To investigate the ability of CFI400945 to effectively penetrate the blood-brain or blood-tumor barriers *in vivo*, xenograft tumors were allowed to establish after injection of patient-derived pGBM cells stably expressing the luciferase reporter into the forebrain striatum and were treated with TMZ or cotreated with TMZ and CFI400945. The results showed that TMZ modestly improved survival and reduced tumor burden (Fig. 7a, b, and c). Combined treatment with TMZ and CFI400945 significantly reduced tumor burden and improved survival (Fig. 7d). The median survival results showed that the of TMZ and CFI400945 cotreatment group (31.5 days) lived significantly longer than the control (20.3 days), and TMZ (25.7 days) groups (Fig. 7e).

Of relevance, we did not observe any physical or behavioral differences between the treatment groups and the control group. Specifically, there were no statistically significant differences in constitutional signs, including animal weights, between the treatment groups and the control group. Histological analysis of the mice did not reveal any deleterious effects of cotreatment of CFI400945 and TMZ in the main organs, including the heart, liver, spleen, lung, and kidneys (Fig. 8). In summary, a PLK4 chemical inhibitor (CFI-400945) capable

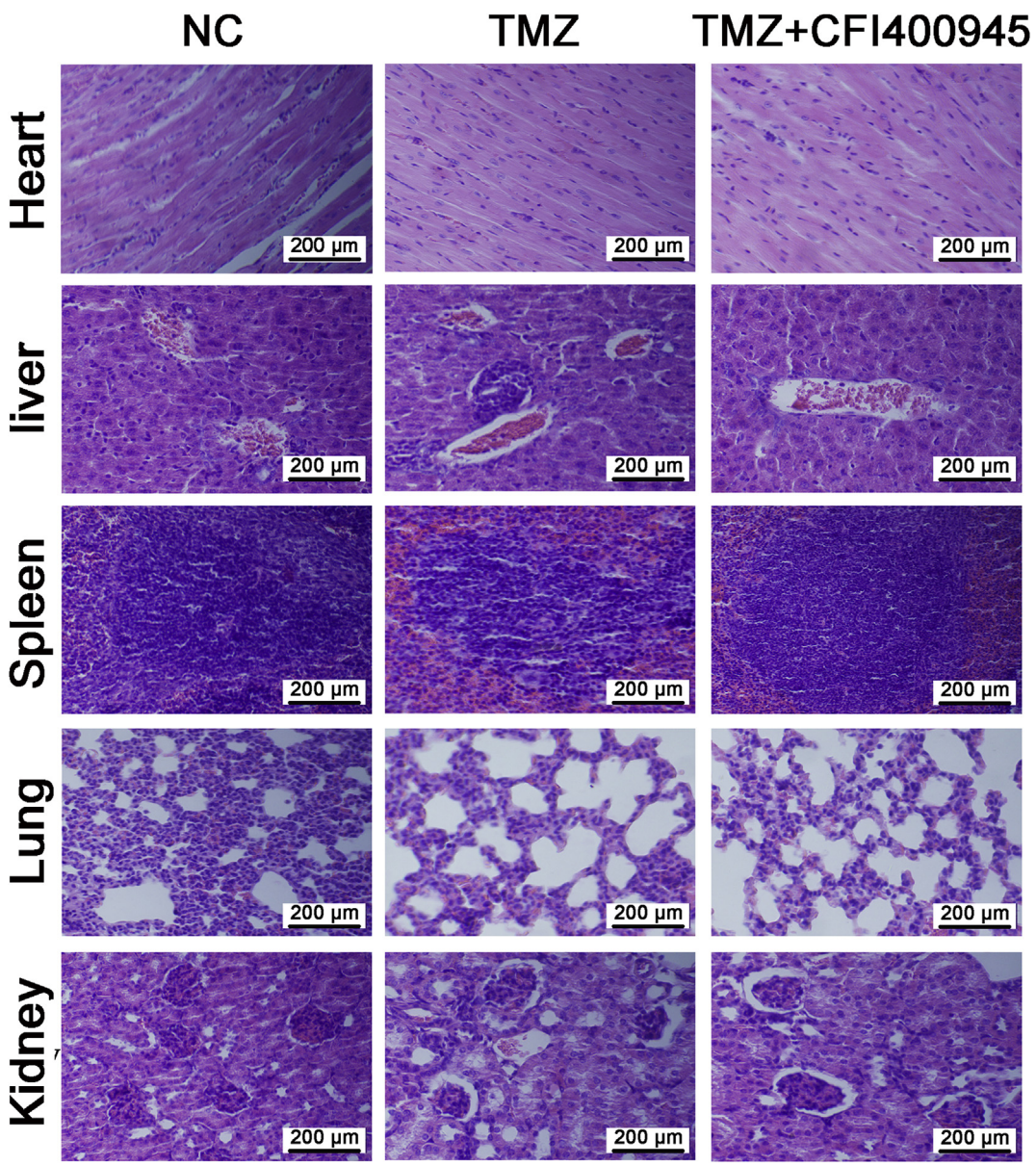

Fig. 8. Images of HE staining of the main organs of mice bearing orthotopic patient-derived primary GBM cells treated with vehicle, TMZ or combination of TMZ and CFI400945. The organs were dissected from mice at three weeks post-implantation.

of effectively penetrating the BBB sensitized patient-derived pGBM cells to TMZ in patient-derived xenograft models, drastically impairing tumor growth and prolonging the survival.

4. Discussion

Collectively, our data describe the PLK4-IKBKE signaling axis that regulates proliferation and the response to chemotherapy in GBM. PLK is known to play a pivotal role in various cell cycle processes to perpetuate proper division [50] and growth of cells [51]. Five mammalian PLK family members have been identified thus far, PLK1, PLK2, PLK3, PLK4 and PLK5 [52]. PLK4 overexpression-related centrosome amplification is considered a direct causative factor for genomic instability and associated tumorigenesis in many cancers [53,54]. However, there are few reports of the biological function of PLK4 in glioma.

First, we showed that the mRNA level of PLK4 was significantly associated with glioma grade and inversely correlated with OS in HGG in four independent cohorts (Fig. 1). The abnormal expression level of PLK4 observed in these cohorts was further verified in glioma samples of different grades via qPCR, suggesting a functional role of PLK4 in the pathogenesis of glioma (Fig. 2). In the CGGA cohort, cluster analysis revealed gene set differences between PLK4 high and low-expressing patients (Fig. 3a), indicating that PLK4 regulated genes involved in cell proliferation and DNA damage repair as determined via GO and KEGG pathway analyses (Fig. 3b–d). These analyses indicated a strong association between PLK4 and chemotherapy, and further analyses indicated that patients with low PLK4 expression levels gained greater survival benefits from alkylating radiochemotherapy than did those with high PLK4 expression levels (Fig. 3e–l). *In vitro* and *in vivo* analysis showed that overexpression of PLK4 sufficed to induce TMZ resistance, whereas inhibition of PLK4 by siRNA overcame the resistance (Fig. 4k–s). Thus, these findings indicate that PLK4 is a crucial factor of chemosensitivity and a valuable prognostic marker in GBM.

Upon stimulus activation, the IKK complex phosphorylates IκBα, marking it for degradation and the subsequent release of NF-κB. Once translocated to the nucleus, NF-κB dimers can regulate the transcription of various genes involved in chemoresistance [55,56] and poor prognosis [57]. Previous results showed that inhibition of IKK-mediated NF-

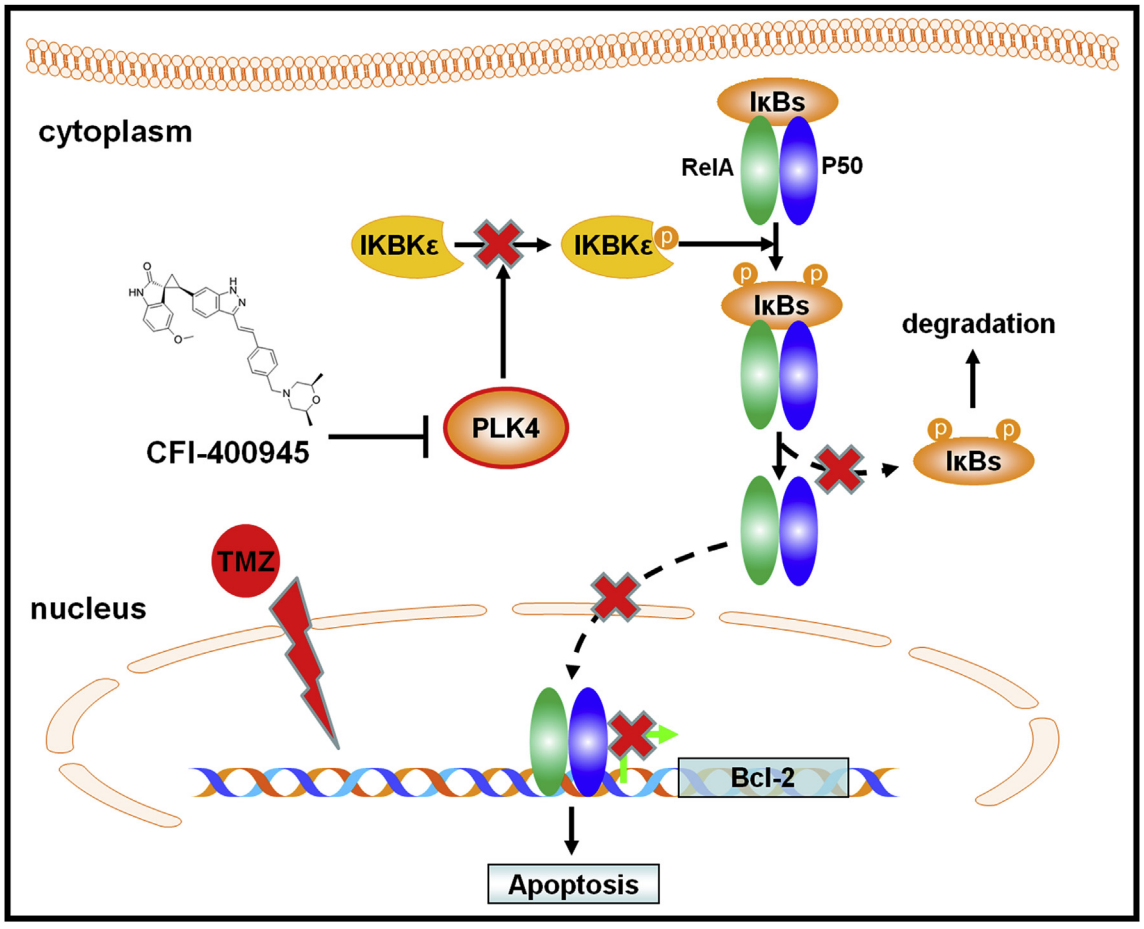

Fig. 9. Diagram representing a proposed model of PLK4 regulation of IKBKE leading to TMZ resistance in GBM.

κB activation suppressed anti-apoptotic factors and activated apoptosis in GBM cells [58–61]. Furthermore, data analysis revealed that IKBKE (a member of the IKK family) might be a potential substrate of PLK4 (data not shown), suggesting a link between PLK4 and IKBKE/NF-κB, which has a critical role in chemosensitivity in GBM. Our data showed that PLK4 interacted with IKBKE and phosphorylated IKBKE *in vitro* and *in vivo* (Fig. 5e–g). Other results have indicated that IKBKE is linked to TMZ chemosensitivity in GBM [61]. We showed that PLK4 phosphorylated IKBKE (Fig. 5h and i), which significantly induced NF-κB transactivation activity and Bcl-2 family expression (Fig. 5c). Notably, overexpression of IKBKE abrogated the effect of PLK4 knockdown on chemosensitivity (Fig. 5j–l). Our data not only reveal the roles of PLK4-IKBKE in GBM chemosensitivity, but also suggest PLK4 as a potential target for treating GBM through pharmacologic inhibition. The amino acid(s) of IKBKE that are phosphorylated by PLK4 are under study in our laboratory. Further studies are needed to characterize the role of phosphorylated IKBKE in PLK4-induced chemoresistance in GBM.

Finally, several small molecule inhibitors of PLK4 kinases, such as CFI400945 [34], and centrinone B [62], have been developed and are currently undergoing preclinical and early clinical testing. CFI400945, discovered in 2013, is the first orally bioavailable PLK4 inhibitor, and has entered phase I clinical trials (NCT01954316) for the treatment of human solid tumors. Notably, CFI400945 elicited antineoplastic effects in breast cancer [63], pancreatic cancer [64], lung cancer [65], rhabdoid tumors and pediatric medulloblastoma [66]. In this report, we showed that CFI400945 cooperated with TMZ in a primary GBM patient-derived subcutaneous xenograft model (Fig. 6). The encouraging antineoplastic findings in the subcutaneous model prompted us to explore the potential for BBB permeability of CFI400945 in the GBM patient-derived orthotopic xenograft model. The results placed it at the cusp of drugs with known *in vivo* BBB penetration sufficient for brain target engagement (Fig. 7). In addition, the major organs in different treatment groups, including heart, liver, spleen, lung, and kidney, were also collected for histopathological analysis, and no pathological changes in the visceral organs could be found in the cotreatment group (Fig. 8). On the basis of the data presented above, CFI400945 is now in early clinical development for use as a promising chemosensitizer in combination with TMZ for the treatment of CNS malignancies.

In conclusion, this study not only describes a signaling axis by which PLK4 phosphorylation of IKBKE contributes to GBM malignancy and lessens tumor response to chemotherapy, but also reveals a clinical opportunity involving a combination of a PLK4 inhibitor and TMZ for treating patients with GBM (Fig. 9). Discovering whether these results are generalizable to the treatment of other cancers will be interesting.

Declarations of interest

None.

Acknowledgements

This work was supported by the grants (Nos. 81773187, 81572496, and 81502306) from the National Nature Science Foundation of China, and a grant (A0101-2018001) from Science and technology projects in key areas of Chinese traditional medicine of Tianjin city. Support was also received from the Tianjin High School Program for Young and Middle-aged Talents Backbone and the Tianjin Young Medical Talents Program. The authors thank Dr. Jinquan Cai (Department of neurosurgery, the second affiliated hospital of harbin medical university, Harbin, Heilong Jiang, China) for assisting the data analysis. We also

thank Dr. Chao Yang and Kaikai Yi (Tianjin Neurological Institute, Tianjin Medical University General Hospital, Tianjin, 300052, China) for facilitating the animal assay. We also acknowledge Dr Weichao Fu (State key laboratory of experimental hematology, Chinese Academy of Medical Sciences, Tianjin, China) for his assistance in living imaging.

References

[1] Z.A. Binder, A.H. Thorne, S. Bakas, E.P. Wileyto, M. Bilello, H. Akbari, S. Rathore, S.M. Ha, L. Zhang, C.J. Ferguson, S. Dahiya, W.L. Bi, D.A. Reardon, A. Idbaih, J. Felsberg, B. Hentschel, M. Weller, S.J. Bagley, J.J.D. Morrissette, M.P. Nasrallah, J. Ma, C. Zanca, A.M. Scott, L. Orellana, C. Davatzikos, F.B. Furnari, D.M. O'Rourke, Epidermal growth factor receptor extracellular domain mutations in glioblastoma present opportunities for clinical imaging and therapeutic development, Cancer Cell 34 (2018) 163–177.

[2] D.S. Hersh, B.G. Harder, A. Roos, S. Peng, J.E. Heath, T. Legesse, A.J. Kim, G.F. Woodworth, N.L. Tran, J.A. Winkles, The TNF receptor family member Fn14 is highly expressed in recurrent glioblastoma and in GBM patient-derived xenografts with acquired temozolomide resistance, Neuro Oncol. 20 (2018) 1321–1330.

[3] T. Huang, C.K. Kim, A.A. Alvarez, R.P. Pangeni, X. Wan, X. Song, T. Shi, Y. Yang, N. Sastry, C.M. Horbinski, S. Lu, R. Stupp, J.A. Kessler, R. Nishikawa, I. Nakano, E.P. Sulman, X. Lu, C.D. James, X.M. Yin, B. Hu, S.Y. Cheng, MST4 phosphorylation of ATG4B regulates autophagic activity, tumorigenicity, and radioresistance in glioblastoma, Cancer Cell 32 (2017) 840–855.

[4] S.H. Chu, S. Karri, Y.B. Ma, D.F. Feng, Z.Q. Li, In vitro and in vivo radiosensitization induced by hydroxyapatite nanoparticles, Neuro Oncol. 15 (2013) 880–890.

[5] W.C. Cho, Targeting the signaling pathways in cancer therapy, Expert Opin. Ther. Targets 16 (2012) 1–3.

[6] T. Ideker, R. Sharan, Protein networks in disease, Genome Res. 18 (2008) 644–652.

[7] W. Kolch, A. Pitt, Functional proteomics to dissect tyrosine kinase signalling pathways in cancer, Nat. Rev. Canc. 10 (2010) 618–629.

[8] B. Chu, A. He, Y. Tian, W. He, Hu J. Chen, R. Xu, W. Zhou, M. Zhang, P. Yang, S.S.C. Li, Y. Sun, P. Li, T. Hunter, R. Tian, Photoaffinity-engineered protein scaffold for systematically exploring native phosphotyrosine signaling complexes in tumor samples, Proc. Natl. Acad. Sci. U. S. A. 115 (2018) E8863–E8872.

[9] C. Arquint, A.M. Gabryjonczyk, S. Imseng, R. Böhm, E. Sauer, S. Hiller, E.A. Nigg, T. Maier, STIL binding to Polo-box 3 of PLK4 regulates centriole duplication, Elife 4 (2015) e07888.

[10] Y. Liu, G.D. Gupta, D.D. Barnabas, F.G. Agircan, S. Mehmood, D. Wu, E. Coyaud, C.M. Johnson, S.H. McLaughlin, A. Andreeva, S.M.V. Freund, C.V. Robinson, S.W.T. Cheung, B. Raught, L. Pelletier, M. van Breugel, Direct binding of CEP85 to STIL ensures robust PLK4 activation and efficient centriole assembly, Nat. Commun. 9 (2018) 1731.

[11] F. Eckerdt, T.M. Yamamoto, A.L. Lewellyn, J.L. Maller, Identification of a polo-like kinase 4-dependent pathway for de novo centriole formation, Curr. Biol. 21 (2011) 428–432.

[12] K. Kazazian, C. Go, H. Wu, O. Brashavitskaya, R. Xu, J.W. Dennis, A.C. Gingras, C.J. Swallow, Plk4 promotes cancer invasion and metastasis through Arp2/3 complex regulation of the actin cytoskeleton, Cancer Res. 77 (2017) 434–447.

[13] X. Tian, D. Zhou, L. Chen, Y. Tian, B. Zhong, Y. Cao, Q. Dong, M. Zhou, J. Yan, Y. Wang, Y. Qiu, L. Zhang, Z. Li, H. Wang, D. Wang, G. Ying, Q. Zhao, Polo-like kinase 4 mediates epithelial-mesenchymal transition in neuroblastoma via PI3K/Akt signaling pathway, Cell Death Dis. 9 (2018) 54.

[14] R. Pellegrino, D.F. Calvisi, S. Ladu, V. Ehemann, T. Staniscia, M. Evert, F. Dombrowski, P. Schirmacher, T. Longerich, Oncogenic and tumor suppressive roles of polo-like kinases in human hepatocellular carcinoma, Hepatology 51 (2010) 857–868.

[15] H. Maamoun, M. Zachariah, J.H. McVey, F.R. Green, A. Agouni, Heme oxygenase (HO)-1 induction prevents Endoplasmic Reticulum stress-mediated endothelial cell death and impaired angiogenic capacity, Biochem. Pharmacol. 127 (2017) 46–59.

[16] R.J. Antonia, A.S. Baldwin, IKK promotes cytokine-induced and cancer-associated AMPK activity and attenuates phenformin-induced cell death in LKB1-deficient cells, Sci. Signal. 11 (2018) pii: eaan5850.

[17] J.D. Phelan, R.M. Young, D.E. Webster, S. Roulland, G.W. Wright, M. Kasbekar, A.L. Shaffer, M. Ceribelli, J.Q. Wang, R. Schmitz, M. Nakagawa, E. Bachy, D.W. Huang, Y. Ji, L. Chen, Y. Yang, H. Zhao, X. Yu, W. Xu, M.M. Palisoc, R.R. Valadez, T. Davies-Hill, W.H. Wilson, W.C. Chan, E.S. Jaffe, R.D. Gascoyne, E. Campo, A. Rosenwald, G. Ott, J. Delabie, L.M. Rimsza, F.J. Rodriguez, F. Estephan, M. Holdhoff, M.J. Kruhlak, S.M. Hewitt, C.J. Thomas, S. Pittaluga, T. Oellerich, L.M. Staudt, A multiprotein supercomplex controlling oncogenic signalling in lymphoma, Nature 560 (2018) 387–391.

[18] J. Yang, F.R. LeBlanc, S.A. Dighe, C.E. Hamele, T.L. Olson, D.J. Feith, T.P. Loughran Jr., TRAIL mediates and sustains constitutive NF-κB activation in LGL leukemia, Blood 131 (2018) 2803–2815.

[19] N. Wang, W. Liu, Y. Zheng, S. Wang, B. Yang, M. Li, J. Song, F. Zhang, X. Zhang, Q. Wang, Z. Wang, CXCL1 derived from tumor-associated macrophages promotes breast cancer metastasis via activating NF-κB/SOX4 signaling, Cell Death Dis. 9 (2018) 880.

[20] L. Sun, Y. Huang, Y. Liu, Y. Zhao, X. He, L. Zhang, F. Wang, Y. Zhang, Ipatasertib, a novel Akt inhibitor, induces transcription factor FoxO3a and NF-κB directly regulates PUMA-dependent apoptosis, Cell Death Dis. 9 (2018) 911.

[21] H. Zhang, Y. Song, H. Yang, Z. Liu, L. Gao, X. Liang, C. Ma, Tumor cell-intrinsic Tim-3 promotes liver cancer via NF-κB/IL-6/STAT3 axis, Oncogene 37 (2018) 2456–2468.

[22] P. Radhakrishnan, V.C. Bryant, E.C. Blowers, R.N. Rajule, N. Gautam, M.M. Anwar, A.M. Mohr, P.M. Grandgenett, S.K. Bunt, J.L. Arnst, S.M. Lele, Y. Alnouti, M.A. Hollingsworth, A. Natarajan, Targeting the NF-κB and mTOR pathways with a quinoxaline urea analog that inhibits IKKβ for pancreas cancer therapy, Clin. Canc. Res. 19 (2013) 2025–2035.

[23] R. Garg, J.M. Blando, C.J. Perez, P. Lal, M.D. Feldman, E.M. Smyth, E. Ricciotti, T. Grosser, F. Benavides, M.G. Kazanietz, COX-2 mediates pro-tumorigenic effects of PKCε in prostate cancer, Oncogene (2018), https://doi.org/10.1038/s41388-018-0318-9.

[24] Y.H. Wu, Y.F. Huang, T.H. Chang, C.Y. Chou, Activation of TWIST1 by COL11A1 promotes chemoresistance and inhibits apoptosis in ovarian cancer cells by modulating NF-κB-mediated IKKβ expression, Int. J. Canc. 141 (2017) 2305–2317.

[25] G. Fianco, M.P. Mongiardi, A. Levi, T. De Luca, M. Desideri, D. Trisciuoglio, D. Del Bufalo, I. Cinà, A. Di Benedetto, M. Mottolese, A. Gentile, D. Centonze, F. Ferrè, D. Barilà, Caspase-8 contributes to angiogenesis and chemotherapy resistance in glioblastoma, Elife 6 (2017) e22593.

[26] L. Wu, G.M. Bernal, K.E. Cahill, P. Pytel, C.A. Fitzpatrick, H. Mashek, R.R. Weichselbaum, B. Yamini, BCL3 expression promotes resistance to alkylating chemotherapy in gliomas, Sci. Transl. Med. 10 (2018) pii: eaar2238.

[27] R. Habedanck, Y.D. Stierhof, C.J. Wilkinson, E.A. Nigg, The Polo kinase Plk4 functions in centriole duplication, Nat. Cell Biol. 7 (2005) 1140–1146.

[28] J. Lu, Y. Yang, G. Guo, Y. Liu, Z. Zhang, S. Dong, Y. Nan, Z. Zhao, Y. Zhong, Q. Huang, IKBKE regulates cell proliferation and epithelial-mesenchymal transition of human malignant glioma via the Hippo pathway, Oncotarget 8 (2017) 49502–49514.

[29] R. Duan, L. Han, Q. Wang, J. Wei, L. Chen, J. Zhang, C. Kang, L. Wang, HOXA13 is a potential GBM diagnostic marker and promotes glioma invasion by activating the Wnt and TGF-β pathways, Oncotarget 6 (2015) 27778–27793.

[30] L. Han, K.L. Zhang, J.X. Zhang, L. Zeng, C.H. Di, B.E. Fee, M. Rivas, Z.S. Bao, T. Jiang, D. Bigner, C.S. Kang, D.C. Adamson, AJAP1 is dysregulated at an early stage of gliomagenesis and suppresses invasion through cytoskeleton reorganization, CNS Neurosci. Ther. 20 (2014) 429–437.

[31] Q. Zheng, L. Han, Y. Dong, J. Tian, W. Huang, Z. Liu, X. Jia, T. Jiang, J. Zhang, X. Li, C. Kang, H. Ren, JAK2/STAT3 targeted therapy suppresses tumor invasion via disruption of the EGFRvIII/JAK2/STAT3 axis and associated focal adhesion in EGFRvIII-expressing glioblastoma, Neuro Oncol. 16 (2014) 1229–1243.

[32] T.A. Barone, C.A. Burkhart, A. Safina, G. Haderski, K.V. Gurova, A.A. Purmal, A.V. Gudkov, R.J. Plunkett, Anticancer drug candidate CBL0137, which inhibits histone chaperone FACT, is efficacious in preclinical orthotopic models of temozolomide- responsive and -resistant glioblastoma, Neuro Oncol. 19 (2017) 186–196.

[33] C. He, J. Li, P. Cai, T. Ahmed, J. Henderson, W. Foltz, R. Bendayan, A. Rauth, X. Wu, Two-step targeted hybrid nanoconstructs increase brain penetration and efficacy of the therapeutic antibody trastuzumab against brain metastasis of HER2-positive breast cancer, Adv. Funct. Mater. 28 (2018) 1705668.

[34] J.M. Mason, D.C. Lin, X. Wei, Y. Che, Y. Yao, R. Kiarash, D.W. Cescon, G.C. Fletcher, D.E. Awrey, M.R. Bray, G. Pan, T.W.3 Mak, Functional characterization of CFI-400945, a Polo-like kinase 4 inhibitor, as a potential anticancer agent, Cancer Cell 26 (2014) 163–176.

[35] R.G. Verhaak, K.A. Hoadley, E. Purdom, V. Wang, Y. Qi, M.D. Wilkerson, C.R. Miller, L. Ding, T. Golub, J.P. Mesirov, G. Alexe, M. Lawrence, M. O'Kelly, P. Tamayo, B.A. Weir, S. Gabriel, W. Winckler, S. Gupta, L. Jakkula, H.S. Feiler, J.G. Hodgson, C.D. James, J.N. Sarkaria, C. Brennan, A. Kahn, P.T. Spellman, R.K. Wilson, T.P. Speed, J.W. Gray, M. Meyerson, G. Getz, C.M. Perou, D.N. Hayes, Integrated genomic analysis identifies clinically relevant subtypes of glioblastoma characterized by abnormalities in PDGFRA, IDH1, EGFR, and NF1, Cancer Cell 17 (2010) 98–110.

[36] Q. Wang, J. Zhang, Y. Liu, W. Zhang, J. Zhou, R. Duan, P. Pu, C. Kang, L. Han, A novel cell cycle-associated lncRNA, HOXA11-AS, is transcribed from the 5-prime end of the HOXA transcript and is a biomarker of progression in glioma, Cancer Lett. 373 (2016) 251–259.

[37] S.M. Evans, K.G. Rodino, H.E. Adcox, J.A. Carlyon, Orientia tsutsugamushi uses two Ank effectors to modulate NF-κB p65 nuclear transport and inhibit NF-κB transcriptional activation, PLoS Pathog. 14 (2018) e1007023.

[38] M.S.1 Brassesco, G.M. Roberto, A.G. Morales, J.C. Oliveira, L.E. Delsin, J.A. Pezuk, E.T. Valera, C.G. Carlotti Jr., E.M. Rego, H.F. de Oliveira, C.A. Scrideli, K. Umezawa, L.G. Tone, Inhibition of NF- κ B by dehydroxymethylepoxyquinomicin suppresses invasion and synergistically potentiates temozolomide and γ-radiation cytotoxicity in glioblastoma cells, Chemother. Res. Pract. 2013 (2013) 593020.

[39] C.Y. Wang, J.C. Cusack Jr., R. Liu, A.S. Baldwin Jr., Control of inducible chemoresistance: enhanced anti-tumor therapy through increased apoptosis by inhibition of NF-kappaB, Nat. Med. 5 (1999) 412–417.

[40] L. Li, Y. Hu, I. Ylivinkka, H. Li, P. Chen, J. Keski-Oja, M. Hyytiäinen, NETRIN-4 protects glioblastoma cells FROM temozolomide induced senescence, PLoS One 8 (2013) e80363.

[41] N. Gaspar, L. Marshall, L. Perryman, D.A. Bax, S.E. Little, M. Viana-Pereira, S.Y. Sharp, G. Vassal, A.D. Pearson, R.M. Reis, D. Hargrave, P. Workman, C. Jones, MGMT-independent temozolomide resistance in pediatric glioblastoma cells associated with a PI3-kinase-mediated HOX/stem cell gene signature, Cancer Res. 70 (2010) 9243–9252.

[42] S. Kohsaka, L. Wang, K. Yachi, R. Mahabir, T. Narita, T. Itoh, M. Tanino, T. Kimura, H. Nishihara, S. Tanaka, STAT3 inhibition overcomes temozolomide resistance in glioblastoma by downregulating MGMT expression, Mol. Canc. Therapeut. 11 (2012) 1289–1299.

[43] L. Wagner, V. Marschall, S. Karl, S. Cristofanon, K. Zobel, K. Deshayes, D. Vucic, K.M. Debatin, S. Fulda, Smac mimetic sensitizes glioblastoma cells to

Temozolomide-induced apoptosis in a RIP1- and NF-κB-dependent manner, Oncogene 32 (2013) 988–997.
[44] S. Haemmig, U. Baumgartner, A. Glück, S. Zbinden, M.P. Tschan, A. Kappeler, L. Mariani, I. Vajtai, E. Vassella, miR-125b controls apoptosis and temozolomide resistance by targeting TNFAIP3 and NKIRAS2 in glioblastomas, Cell Death Dis. 5 (2014) e1279.
[45] J.C. Loftus, H. Dhruv, S. Tuncali, J. Kloss, Z. Yang, C.A. Schumacher, B. Cao, B.O. Williams, J.M. Eschbacher, J.T. Ross, N.L. Tran, TROY (TNFRSF19) promotes glioblastoma survival signaling and therapeutic resistance, Mol. Canc. Res. 11 (2013) 865–874.
[46] S. Caporali, L. Levati, G. Graziani, A. Muzi, M.G. Atzori, E. Bonmassar, G. Palmieri, P.A. Ascierto, S. D'Atri, NF-κB is activated in response to temozolomide in an AKT-dependent manner and confers protection against the growth suppressive effect of the drug, J. Transl. Med. 10 (2012) 252.
[47] M. Rajurkar, K. Dang, M.G. Fernandez-Barrena, X. Liu, M.E. Fernandez-Zapico, B.C. Lewis, J. Mao, IKBKE is required during KRAS-induced pancreatic tumorigenesis, Cancer Res. 77 (2017) 320–329.
[48] T. Shimada, T. Kawai, K. Takeda, M. Matsumoto, J. Inoue, Y. Tatsumi, A. Kanamaru, S. Akira, IKK-i, a novel lipopolysaccharide-inducible kinase that is related to IkappaB kinases, Int. Immunol. 11 (1999) 1357–1362.
[49] C.F. Cho, J.M. Wolfe, C.M. Fadzen, D. Calligaris, K. Hornburg, E.A. Chiocca, N.Y.R. Agar, B.L. Pentelute, S.E. Lawler, Blood-brain-barrier spheroids as an in vitro screening platform for brain-penetrating agents, Nat. Commun. 8 (2017) 15623.
[50] S.A.G. Cuijpers, A.C.O. Vertegaal, Guiding mitotic progression by crosstalk between post-translational modifications, Trends Biochem. Sci. 43 (2018) 251–268.
[51] G. de Cárcer, P. Wachowicz, S. Martínez-Martínez, J. Oller, N. Méndez-Barbero, B. Escobar, A. González-Loyola, T. Takaki, A. El Bakkali, J.A. Cámara, L.J. Jiménez-Borreguero, X.R. Bustelo, M. Cañamero, F. Mulero, M. de Los Ángeles Sevilla, M.J. Montero, J.M. Redondo, M. Malumbres, Plk1 regulates contraction of post-mitotic smooth muscle cells and is required for vascular homeostasis, Nat. Med. 23 (2017) 964–974.
[52] K. Strebhardt, Multifaceted polo-like kinases: drug targets and antitargets for cancer therapy, Nat. Rev. Drug Discov. 9 (2010) 643–660.
[53] M.S. Levine, B. Bakker, B. Boeckx, J. Moyett, J. Lu, B. Vitre, D.C. Spierings, P.M. Lansdorp, D.W. Cleveland, D. Lambrechts, F. Foijer, A.J. Holland, Centrosome amplification is sufficient to promote spontaneous tumorigenesis in mammals, Dev. Cell 40 (2017) 313–322.
[54] Ö. Serçin, J.C. Larsimont, A.E. Karambelas, V. Marthiens, V. Moers, B. Boeckx, M. Le Mercier, D. Lambrechts, R. Basto, C. Blanpain, Transient PLK4 overexpression accelerates tumorigenesis in p53-deficient epidermis, Nat. Cell Biol. 18 (2016) 100–110.
[55] Y. Zhang, L. Zhang, Y. Hu, K. Jiang, Z. Li, Y.Z. Lin, G. Wei, W. Lu, Cell-permeable NF-κB inhibitor-conjugated liposomes for treatment of glioma, J. Contr. Release 289 (2018) 102–113.
[56] K.M. Dhandapani, V.B. Mahesh, D.W. Brann, Curcumin suppresses growth and chemoresistance of human glioblastoma cells via AP-1 and NFkappaB transcription factors, J. Neurochem. 102 (2007) 522–538.
[57] K.P.L. Bhat, V. Balasubramaniyan, B. Vaillant, R. Ezhilarasan, K. Hummelink, F. Hollingsworth, K. Wani, L. Heathcock, J.D. James, L.D. Goodman, S. Conroy, L. Long, N. Lelic, S. Wang, J. Gumin, D. Raj, Y. Kodama, A. Raghunathan, A. Olar, K. Joshi, C.E. Pelloski, A. Heimberger, S.H. Kim, D.P. Cahill, G. Rao, W.F.A. Den Dunnen, H.W.G.M. Boddeke, H.S. Phillips, I. Nakano, F.F. Lang, H. Colman, E.P. Sulman, K. Aldape, Mesenchymal differentiation mediated by NF-κB promotes radiation resistance in glioblastoma, Cancer Cell 24 (2013) 331–346.
[58] S. Karmakar, N.L. Banik, S.K. Ray, Curcumin suppressed anti-apoptotic signals and activated cysteine proteases for apoptosis in human malignant glioblastoma U87MG cells, Neurochem. Res. 32 (2007) 2103–2113.
[59] J.U. Jung, S. Ravi, D.W. Lee, K. McFadden, M.L. Kamradt, L.G. Toussaint, R. Sitcheran, NIK/MAP3K14 regulates mitochondrial dynamics and trafficking to promote cell invasion, Curr. Biol. 26 (2016) 3288–3302.
[60] G.R. Sareddy, K. Geeviman, C. Ramulu, P.P. Babu, The nonsteroidal anti-inflammatory drug celecoxib suppresses the growth and induces apoptosis of human glioblastoma cells via the NF-κB pathway, J. Neuro Oncol. 106 (2012) 99–109.
[61] H. Guan, H. Zhang, J. Cai, J. Wu, J. Yuan, J. Li, Z. Huang, M. Li, IKBKE is overexpressed in glioma and contributes to resistance of glioma cells to apoptosis via activating NF-κB, J. Pathol. 223 (2011) 436–445.
[62] Y.L. Wong, J.V. Anzola, R.L. Davis, M. Yoon, A. Motamedi, A. Kroll, C.P. Seo, J.E. Hsia, S.K. Kim, J.W. Mitchell, B.J. Mitchell, A. Desai, T.C. Gahman, A.K. Shiau, K. Oegema, Cell biology. Reversible centriole depletion with an inhibitor of Polo-like kinase 4, Science 348 (2015) 1155–1160.
[63] P.B. Sampson, Y. Liu, B. Forrest, G. Cumming, S.W. Li, N.K. Patel, L. Edwards, R. Laufer, M. Feher, F. Ban, D.E. Awrey, G. Mao, O. Plotnikova, R. Hodgson, I. Beletskaya, J.M. Mason, X. Luo, V. Nadeem, X. Wei, R. Kiarash, B. Madeira, P. Huang, T.W. Mak, G. Pan, H.W. Pauls, The discovery of Polo-like kinase 4 inhibitors: identification of (1R,2S).2-(3-((E).4-(((cis).2,6-dimethylmorpholino)methyl)styryl).1H.indazol-6-yl)-5'- methoxyspiro[cyclopropane-1,3'-indolin]-2'-one (CFI-400945) as a potent, orally active antitumor agent, J. Med. Chem. 58 (2015) 147–169.
[64] I. Lohse, J. Mason, P.M. Cao, M. Pintilie, M. Bray, D.W. Hedley, Activity of the novel polo-like kinase 4 inhibitor CFI-400945 in pancreatic cancer patient-derived xenografts, Oncotarget 8 (2017) 3064–3071.
[65] M. Kawakami, L.M. Mustachio, L. Zheng, Y. Chen, J. Rodriguez-Canales, B. Mino, J.M. Kurie, J. Roszik, P.A. Villalobos, K.L. Thu, J. Silvester, D.W. Cescon, Wistuba II, T.W. Mak, X. Liu, E. Dmitrovsky, Polo-like kinase 4 inhibition produces polyploidy and apoptotic death of lung cancers, Proc. Natl. Acad. Sci. U. S. A. 115 (2018) 1913–1918.
[66] S.T. Sredni, A.W. Bailey, A. Suri, R. Hashizume, X. He, N. Louis, T. Gokirmak, D.R. Piper, D.M. Watterson, T. Tomita, Inhibition of polo-like kinase 4 (PLK4): a new therapeutic option for rhabdoid tumors and pediatric medulloblastoma, Oncotarget 8 (2017) 111190–111212.